TECHNISCHE UNIVERSITÄT WIEN



Validierung des Festigkeitsverhaltens eines menschlichen Lung-on-Chip-Modells bei Beatmung

DIPLOMARBEIT

zur Erlangung des akademischen Grades

Diplom-Ingenieur

im Rahmen des Studiums

Biomediziningenieurwesen

eingereicht von

Laurin Hildebrandt, B.Eng.

an der Fakultät für Technische Chemie

der Technischen Universität Wien

Betreuung: Univ. Prof. Dipl.-Ing. Dr. Peter Ertl, Vizerektor für Forschung, Innovation und Internationales

Mitwirkung: Dr. Martin Frauenlob, Senior Scientist

Wien, 12. Mai 2025

Laurin Hildebrandt

Peter Ertl





Assessing Mechanical Stimulation in a Human Lung Alveolus-on-chip Model under Respiratory Conditions

DIPLOMA THESIS

submitted in partial fulfilment of the requirements for the degree of

Master of Science

in

Biomedical Engineering

by

Laurin Hildebrandt, B.Eng.

to the Faculty of Technical Chemistry

at the TU Wien

Advisor: Univ. Prof. Dipl.-Ing. Dr. Peter Ertl, Vizerektor für Forschung, Innovation und Internationales

Assistance: Dr. Martin Frauenlob, Senior Scientist

Vienna, May 12, 2025

Laurin Hildebrandt

Peter Ertl



TU **Bibliothek**, Die approbierte gedruckte Originalversion dieser Diplomarbeit ist an der TU Wien Bibliothek verfügbar wien knowledgehub. The approved original version of this thesis is available in print at TU Wien Bibliothek.

Erklärung zur Verfassung der Arbeit

Laurin Hildebrandt, B.Eng.

Hiermit erkläre ich, dass ich diese Arbeit selbständig verfasst habe, dass ich die verwendeten Quellen und Hilfsmittel vollständig angegeben habe und dass ich die Stellen der Arbeit - einschließlich Tabellen, Karten und Abbildungen -, die anderen Werken oder dem Internet im Wortlaut oder dem Sinn nach entnommen sind, auf jeden Fall unter Angabe der Quelle als Entlehnung kenntlich gemacht habe.

Wien, 12. Mai 2025

Laurin Hildebrandt

TU Sibliothek, Die appro

Danksagung

Im Rahmen dieser Arbeit gilt mein ausgesprochener Dank Frau PhD cand. Mona Amiratashani. Sie gab mir am Universitätsklinikum Jena nicht nur Zugang zu den praktischen Fertigkeiten im Umgang mit Zellkulturen. Ihr Bestreben äußerte sich im besonderen Maß in der uneigennützigen Wissensvermittlung und der praxisnahen Erkenntnissuche auf Augenhöhe. Dem restlichen Kollegium der Arbeitsgruppe Inspire danke ich für die angebotene, un-bedingte Hilfsbereitschaft. Des Weiteren möchte ich Herrn Professor Peter Ertl sowie Herrn Dr. Martin Frauenlob für die reibungslose Betreuung an der Technischen Universität Wien danken. Ohne die TU gäbe es diese Arbeit nicht, weswegen ich das Mindestmaß an Erwähnung im Folgenden nicht auslassen möchte. An der TU in Wien durfte ich im Kontext meines höchst interdisziplinären Studiengangs einerseits anregende Einblicke in alle acht Fakultäten erhalten, wobei die Veranstaltungen der Professoren Thurner (Biomechanik), Stampfl (Biomaterialien) oder Heuer (Baumechanik) in meiner Spezialisierungsrichtung in ihrer Vortragsweise herausragten. Andererseits bin ich vordergründig der fördernden und sehr responsiven Art meines Dekans, Herrn Professor Eugenjius Kaniusas, dankbar verbunden. Der Studienkatalog bietet eine große Tür zur Initiative, die ich auch dank ihm glücklich für die Einblicke in die Bionik, Frau Professorin Helga Lichtenegger (Universität für Bodenkultur Wien), Gerichtsmedizin, Herr Professor Manfred Hochmeister (Medizinische Universität Wien) oder Technologie und Ethik, Herr PhD cand. Jesse De Pagter, geöffnet habe. Die Belegung von Restmodulen an der Bauhaus-Universität in Weimar verdanke ich ebenso jenem Herrn Professor Kaniusas, der auch die äußerst inspirierenden Auslandssemester in Italien ermöglichte. Neben kulturellen Reizen hinterließ dort die einbeziehende, wissenschaftsbegeisternde Art von Herrn Professor Mattia Veronese (Universität zu Padua) eine bleibende universitäre Erinnerung. Auch Frau Professorin Francesca Susin (ebenfalls Universität zu Padua) und Herr Professor Paolo Netti (Universität zu Neapel) tragen einen erfreulichen Anteil dieser Episode der ausführlichen Semesterprojekte.

Die Aufnahme zum konsekutiven Studium an der TU Wien wäre ohne die Ernst-Abbe-Hochschule Jena, deren Laboringenieure und Frau Professorin Jane Neumann nicht möglich gewesen. Dank ihrer vermittelnden Unterstützung hat sich mit den ersten beiden Auslandssemestern in Tallinn

und Brünn die Tür zum Aufbruch geöffnet. Ein Dank an Herrn Professor Jiri Bursa (Technische Universität Brünn), Herrn Vaclav Havlicek (damalig Weltraumunternehmen S.A.B. Aerospace; meine Erasmus-Praktikumstelle), darf für die inspirierende Betreuung in einer pandemieträchtigen Zeit nicht fehlen. Frau Friedemann und Frau Siegfried vom EU-Praktikum Thüringen ermöglichten diesen Aufenthalt in der damaligen Ungewissheit überhaupt erst.

So führt eine Tür zur nächsten und schließlich stehen wir wieder an der Schwelle zur ersten: Zum Ende der Studienzeit durfte ich die vorliegende Diplomarbeit in Kooperation mit der Arbeitsgruppe von Herrn Professor Iwan Schie an genannter Ernst-Abbe-Hochschule in Jena anfertigen. In beeindruckender Zeit etablierte er dort eine Forschungsinitiative, deren Wissen-Schaffende Strebsamkeit die Perspektive meines damaligen Grundstudiums definitiv auch erweitert hätte. Vielen Dank an PhD cand. Calvin Kreft, der mich für die OCT-Messungen bedingungslos, mitdenkend und ergebnisoffen unterstützte. Mögliche Publikationen meiner Arbeitsgruppe am Universitätsklinikum Jena sollten in jedem Fall seine Nennung finden. Nicht zuletzt danke ich Herrn Professor Sören Kliem und seinem Assistenten Herrn PhD cand. Sebastian Fischer für die Förderung während der entbehrungsreichen Zeit der Diplomarbeit in Form von Wohnraum. Anderweitig wäre dieser Abschnitt nur äußerst kompromissreich überbrückt worden. Abschließend: Vielen Dank an meine Familie und das satte Volumen an umgebender Freundschaft für die vielfältige Begleitung. Auch das etwaige Redigieren der Arbeit weiß ich zu schätzen.

Vor etwa hundert Jahren kippte die Waage der technischen Errungenschaften: Das Verständnis des Einzelnen über die konkrete Funktionsweise aller nutzbaren Dinge wich zunehmend einer un-bewussten Anwendung. Mitunter der Komplexität geschuldet. Ich bin froh, dass ich – selbst im Vergleich mit meinen prägenden, ingenieurtechnisch arbeitenden Großvätern, die komplexe technische Sachverhalte in hochgradig repetitiven, aber sehr bewussten Prozessen zu Papier bringen mussten – heute freier in Zeit, Ort und Methodik handeln kann. Damit steigen freilich auch die Anforderungen; umso dankbarer bin ich für das noch sorgfältige – und damit organische – Lernen während meiner expliziten Studien-Zeit. Besonders im letzten Jahr dieser Arbeit konnte ich beobachten, wie sich die Möglichkeiten zur schnellen Wissenskumulierung erhöhten, während geistige Durststrecken durch das bloße Eintippen kaum noch anregende, oasenfreie Abschnitte hinterließen. Da, auch bedingt durch das Genannte, die Kommunikation zweier Fachdisziplinen im Umfeld dieser Arbeit schleppend verlief und die jeweilige Expansion der Aufgabenbereiche manchmal ohne gemeinsame Schnittmenge erfolgte, möchte ich diese Arbeit als kompakte und erklärende Dokumentation verstehen. Ich hoffe, dass dieser Ansatz beim Lesen erkennbar wird.

The approved original version of this thesis is available in print at

Kurzfassung

Die mechanische Mikroumgebung spielt eine entscheidende Rolle bei der Regulation des Zellverhaltens, insbesondere in dynamischen physiologischen Prozessen wie der Atmung.

Das Ziel dieser Arbeit ist es, die Auswirkungen des durch den Atemmechanismus ausgeübten Drucks auf die zelluläre Dehnung und die Permeabilität in einem neuartigen Lung-on-chip-Modell zu untersuchen. Dies ermöglicht es, das Modell als zuverlässiges Werkzeug für die Erforschung mechanobiologischer Eigenschaften und Reaktionen auf Infektionsmodelle einzusetzen. Für die Validierung werden zunächst mehrere Proben des Lung-on-Chip-Modells hergestellt (Physiologisch vergleichbare extrazelluläre Matrix, Lungen- und Endothelzellen).

Daraufhin wird das Modell mechanisch durch eine definierte Beatmung stimuliert, wobei darauf geachtet wird, dass die Zellviabilität erhalten bleibt, mittels Vital-Fluoreszenz-Doppelfärbung. Dabei wird die Deformation der zellentragenden, organischen Matrix mithilfe der optischen Kohärenzmikroskopie untersucht. Diese Methode ermöglicht es, hochauflösende Bilder des Gewebes zu erhalten und die Struktur sowie die Matrixintegrität zu bewerten. Die Studie verdeutlicht die zellulären Reaktionen auf mechanische Reize, was das Verständnis der Lungenphysiologie während einer Infektion erheblich verbessert.

TU Bibliothek, Die approbierte gedruckte Originalversion dieser Diplomarbeit ist an der TU Wien Bibliothek verfügbar wien vour knowledge hub The approved original version of this thesis is available in print at TU Wien Bibliothek.

Abstract

The mechanical micro-environment plays a crucial role in regulating cellular behaviour and function, particularly in dynamic physiological processes such as breathing.

In this study, we aim to investigate the effects of applied pressure by the breathing mechanism on cellular strain and permeability in a novel lung-on-chip model. This enables the utilization of the model as a reliable tool for investigating mechanobiological properties and responses to infection models. For validation, multiple samples of the lung-on-chip model are initially prepared (physiologically relevant extracellular matrix, lung and endothelial cells).

Afterwards, the model is mechanically stimulated through defined breathing, while ensuring that cell viability is maintained via a live-dead assay. The deformation of the cell-bearing organic matrix is then examined using optical coherence microscopy. This method allows for highresolution images of the tissue, enabling evaluation of the structure and integrity of the matrix. This comprehensive approach illustrates cell responses to mechanical stimuli, which enhances our understanding of lung physiology remarkably during infection.

Contents

Kı	Kurzfassung Abstract Contents								
Al									
Co									
1	Intr	oduction	n	1					
	1.1	Lung F	Physiology and Translation to Modelling	1					
	1.2	Definit	tions	3					
		1.2.1	Stress	3					
		1.2.2	Strain	4					
		1.2.3	Elasticity	4					
		1.2.4	Experiment Conditions during Cyclic Breathing	5					
	1.3	The M	odel and Its Assumptions	5					
	1.4	Scope	of the Thesis	7					
2	Materials and Methods								
	2.1	Produc	ction of Biological Membrane	9					
	2.2	Cells .		10					
		2.2.1	Cell Culture	11					
		2.2.2	Cell Seeding	11					
	2.3	Cyclic	breathing	11					
	2.4	Result	Acquisition	12					
		2.4.1	OCT	12					
		2.4.2	Mechanical Assumptions	15					
		2.4.3	Processing Steps	18					
		2.4.4	Permeability	20					
		2.4.5	Viability	21					
				xiii					

3	Resu	ults	25			
	3.1	Trials	25			
	3.2	OCT	26			
		3.2.1 General remarks	26			
		3.2.2 Pre-tests	29			
		3.2.3 Main Tests	29			
	3.3	Permeability	35			
		3.3.1 Analysis Across All Experiments	35			
		3.3.2 Identical Experimental Conditions	36			
	3.4	Viability	37			
4	Disc	eussion	39			
	4.1	Limitations	43			
5	Sum	nmary	45			
A	App	endix	i			
	A.1	Protocol of Membrane Production	i			
	A.2	Cells	iii			
	A.3	Supportive Microscopy	vi			
	A.4	OCT System Description	vii			
	A.5	Code for <i>TIFF</i> File Processing	vii			
	A.6	OCT Images	xii			
		A.6.1 Pre-tests	xii			
		A.6.2 Main Tests	xiv			
	A.7	Viability	xxvi			
		A.7.1 Orthogonal Projections	xxvi			
		A.7.2 Colour-Coded Projections	xxviii			
Li	st of I	Figures	xxxi			
Li	st of T	Tables	xxxii			
Gl	Glossary					
Ri	Bibliography					

CHAPTER

Introduction

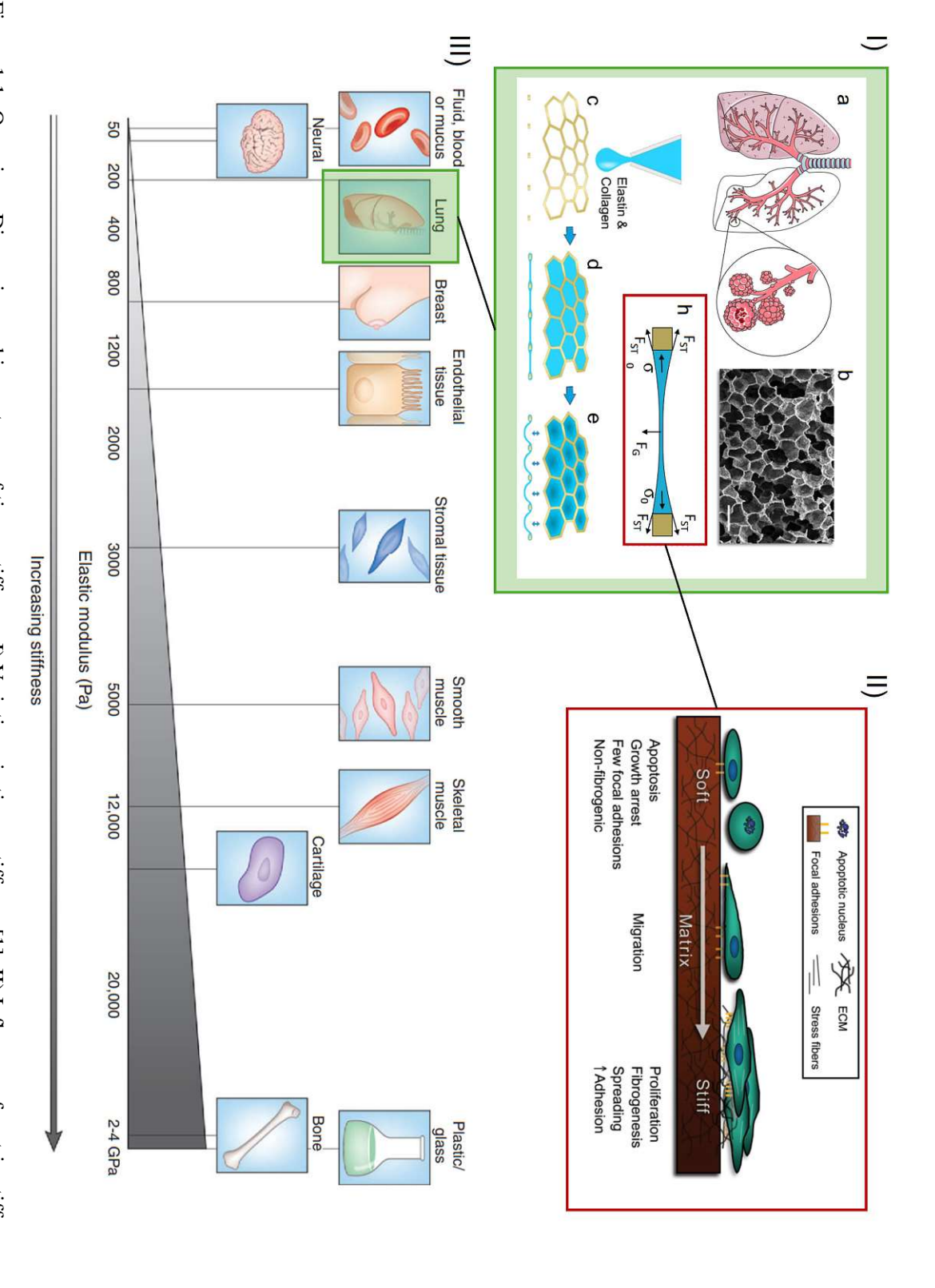
Lung Physiology and Translation to Modelling 1.1

Approximately 24 m³ of air — comparable to the volume of a moderate swimming pool — flows through the lungs of an average adult male with moderate activity daily [4]. Beyond enabling oxygen exchange, the lungs also serve as entry points for airborne pathogens, including the SARS-CoV-2 virus, which specifically targets alveolar type II cells ¹ [5]. The recent global health and economic impact of a respiratory infection highlights the urgent need to better understand lung pathophysiology for advancing therapeutic development.

The human lung is designed to optimize gas exchange by maximizing the surface area while minimizing the diffusion distance. The total alveolar surface area in a healthy adult lung is approximately 140 m³, with a diffusion barrier thickness of 2 µm [6]. This large exchange surface is maintained by a dense capillary network embedded in the inter-alveolar septa, which ensures close proximity between air and blood [7, 8]. Integrating biologically relevant mechanical properties and allowing dynamic ventilation cycles, lung-on-a-chip models serve as a valuable platform for studying lung physiology, disease mechanisms, and drug interactions under realistic conditions, at this air-blood interface.

Traditional in vitro models often fail to replicate the complex micro-environment of the lung, particularly the mechanical stresses induced by respiration. While animal models provide some physiological insights, they often lack human-specific responses and raise ethical concerns [9]. To address these limitations, organ-on-a-chip technology has emerged as a promising alternative. These micro-fluidic devices mimic key aspects of human organ physiology, allowing for controlled

¹Alveolar type II cells will replace the H441 cells in a later phase of this experiment



on cell behaviour[2]. III) Physiology to Modelling: a) Schematic of the respiratory tree-like structure ending with alveolar sacs. b SEM Figure 1.1: Overview: Dimension and importance of tissue stiffness: I) Variations in tissue stiffness [1]. II) Influence of matrix stiffness membrane. F_{ST} , F_G and σ_o stand for surface tension force, gravity and residual stress, respectively. Adapted by [3]. membrane. e) The collagen-elastin gel forms a suspended, stretchable layer. f) Schematic of the force balance during the drying of the picture of a slice of human lung parenchyma with lung alveoli and their air-blood barrier. c, d) Schematic of the production of the CE

studies of lung mechanics, cellular responses, and disease progression under dynamic conditions [10, 3]. Understanding the biomechanical properties of lung tissue under both physiological and pathological conditions is essential for the advancement of respiratory medicine [11]. Tissue is composed of cells and the supportive structure - the Extra-Cellular Matrix (ECM), further called Matrix, (fig. 1.1²).

Hydrogels have gained significant interest for replicating the chemical composition and structure of the native ECM in lung cell culture models due to their mechanical tunability, porosity, and bio-active properties [12]. However, fabricating thin, stretchable hydrogel membranes that can endure cyclic mechanical strain while maintaining physiological cell-matrix interactions remains technically challenging [3]. During breathing, this delicate structure is exposed to heterogeneous mechanical strain, with local deformations influenced by the thickness of the interstitial space and the variable stiffness of lung compartments, as even the mechanical properties of the lung vary significantly across different anatomical compartments. The target region—the alveolar parenchyma³—is the most compliant region, allowing for efficient deformation [7, 13]. Although the model successfully replicates physiological pressures and strain ranges, the membrane thickness of approximately $100 \, \mu m$ substantially exceeds that of the native alveolar barrier (about $2 \, \mu m$), impacting diffusion dynamics and strain localisation.

In this study, a Collagen-Elastin (CE) membrane was developed as a biomimetic model system, inspired by a previous approach⁴. The membrane replicates key biochemical and mechanical features of the alveolar barrier. Collagen type I—the most abundant collagen type in lung tissue [14]—provides essential structural stability, while elastin imparts the elasticity required to endure the continuous deformations associated with breathing cycles.

1.2 Definitions

Before introducing the model, it is necessary to establish some core definitions to facilitate understanding from both physical and biological perspectives.

1.2.1 Stress

Mechanical stress (σ) describes the internal force per unit area within a material subjected to an external load. In the context of this experiment, stress is induced by *mechanical stimulation*

²Note to Figure III: A squared net instead of hexagon is used as a scaffold in our study

³organ-specific tissue composed of cells and intercellular spaces

⁴Zamprogno et al., "Second-generation lung-on-a-chip with an array of stretchable alveoli made with a biological membrane", 2021

through pressure-driven ventilation of the membrane. This process leads to a measurable elastic deflection of the membrane surface.

$$\sigma = \frac{F}{A},\tag{1.1}$$

where F is the applied force [N] and A is the cross-sectional area $[m^2]$. The resulting stress is expressed in Pascals [Pa], where $1 \text{ Pa} = 1 \text{ Nm}^{-2}$.

In this experiment, stress is applied by an orthogonal pressure in the range of millibar [mbar] across the circular area of the membrane-covered mesh (fig. 2.8), corresponding to an overpressure relative to atmospheric pressure. The unit conversion is given by 1 mbar = 100 Pa.

1.2.2 Strain

Strain (ε) quantifies the relative deformation of a material under applied stress. It is defined as the change in length (stretch or displacement) ΔL relative to the original length L_0 :

$$\varepsilon = \frac{\Delta L}{L_0}.\tag{1.2}$$

Strain is a dimensionless quantity, often expressed as a percentage.

1.2.3 **Elasticity**

The stiffness of a component describes how much it deflects under a given load. This depends on the Young's modulus (Elastic modulus) of the material, but also on how it is loaded (tension or bending) and the geometry of the component. Young's modulus measures the resistance of a material to elastic (recoverable) deformation under load (stress to strain). Young's modulus is given by:

$$E = \frac{\sigma}{\varepsilon} \tag{1.3}$$

A stiff material thus has a high Young's modulus. The unit is Pascals.

The stiffness varies significantly across different organs and tissues and is closely linked to their function. Tissues that experience minimal mechanical stress, such as the brain, or highly flexible tissues like the lungs, have low stiffness. In contrast, tissues subjected to substantial mechanical loads, such as bone or skeletal muscle, possess elastic moduli with stiffness levels that are several

TU Sibliothek, WLEN Your knowledge hub

orders of magnitude higher [1], ref. 1.1. The elastic modulus of the alveolar parenchyma is approximately 1-5 kPa [15, 16].

The terms *mechanical stimulation*, *ventilation*, *dynamic loading* and *cyclic breathing* are used as synonyms in respect to stress in this thesis.

1.2.4 Experiment Conditions during Cyclic Breathing

Three experimental conditions (fig. 1.2) are applied to compare the elastic behaviour. During the period, all wells rest in the incubator:

Dynamic: The Well containing the biological membrane **with** epithelial and endothelial cells is exposed to cyclic breathing for 3 days.

Static: The well containing the biological membrane **with** epithelial and endothelial cells is not exposed to cyclic breathing, but stays at rest during the 3 days. *Stat-yes* is used as a synonym.

Control: The well containing the biological membrane and without cells stays at rest during the 3 days. *Stat-no* is used as a synonym.

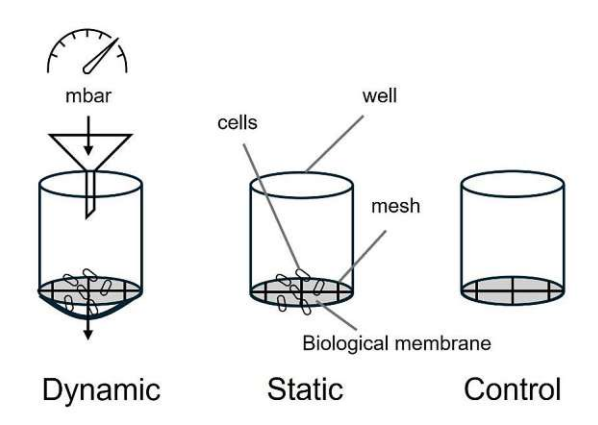


Figure 1.2: Experiment conditions during cyclic breathing

1.3 The Model and Its Assumptions

The experimental design was tailored to replicate key physiological conditions of the alveolar barrier:

• Alveolar-scale architecture: The chip incorporates a net scaffold that suspends the CE membrane within small, square-shaped alcoves. Each alcove, with a diameter of approximately 75 µm, mirrors the size scale of human alveoli (100–200 µm) [13, 17, 18].

TU Sibliothek, Week Your knowledge hub

- **Alveolar-wall-scale architecture:** The supporting polyester mesh divides the alveolus-mimicking chambers, thereby structurally imitating the alveolar walls that stabilise the lung parenchyma [16, 19].
- **Composition:** The membrane consists of lung ECM proteins, specifically collagen and elastin, providing both stretchability and biodegradability. The membrane remains mechanically stable for at least three weeks under standard culture conditions [3].

Together, these architectural and compositional features ensure that the model closely mimics the mechanical and biological environment of the alveolar microstructure.

The following assumptions are examined in this study:

Box 0: Theses

- Realistic breathing mechanics: The collagen-elastin composition enables the recreation of alveolar breathing cycles (10% strain [13, 7]). For the corresponding pressure [20], the elastic modulus is in the range of kilo-pascals[15, 16].
- Physiological strain distribution: The system distributes mechanical stress in a physiological gradient, ensuring that cells experience region-specific deformations, as seen *in vivo*.
- Influence of cells on mechanics: Lower strain levels are reached after epithelial and endothelial cells are added to the biological membrane. This highlights the interplay between tissues and cells.
- Cellular strain: Beyond evaluating the biological membrane, the Optical Coherence Tomography technique allows to study cellular strain. This serves as a proof to validate.
- Influence of cells on permeability: The biological membranes show lower permeability levels when carrying confluent cell layers.

TU Sibliothek, Wurknowledge hub

1.4 Scope of the Thesis

The lung-on-chip project aims to provide insights into the effects of mechanical stimulation on infectious processes at the alveolar site. This master's thesis focuses on characterising the mechanical properties of the biological tissue model. Using OCT⁵, the relationship between applied pressure and membrane strain is investigated. OCT is a high-resolution interferometric imaging technique that employs near-infrared light to visualise micrometer-scale structures with a penetration depth of several millimetres [21].

At the outset of the project, no previous application of OCT in the context of lung mechanics was known. Complementary permeability and viability assays were conducted to broaden the scope of analysis.

➤ A particular strength of OCT — its ability to measure membrane deformation both live and non-invasively — is considered a cornerstone of this work.

The biological component of the project follows protocols established by my colleague Mona Amiratashani (Universitätsklinikum Jena(UKJ)), which are documented in the appendix. As the production of the biological membrane was also required for mechanical characterisation, the entire process, carried out by the author, is described stepwise in the Materials and Methods section.

In a bottom-up approach, the biological membrane is initially assembled. Following successful replication of this step, the membranes are characterised using OCT and the experimental conditions are evaluated. In parallel, epithelial and endothelial cells are cultured and subsequently seeded onto the biological membranes. This experimental set-up is then subjected to mechanical stimulation, achieved through sinusoidal, breathing-like pressure actuation provided by the pump system, developed by a project partner [22]. The adoption of cell culture protocols, the establishment of mechanical stimulation, and the successful implementation of permeability and viability assays form the basis for the integration of the experimental components. Ultimately, after the successful OCT characterisation of cell-free membranes, the co-cultured epithelial and endothelial cell layers are evaluated under mechanical stimulation using OCT to assess strain development.

A critical reflection of the model limitations is provided in the discussion section to contextualise the experimental results.

⁵Also referred to as the 'ultrasound of light'.



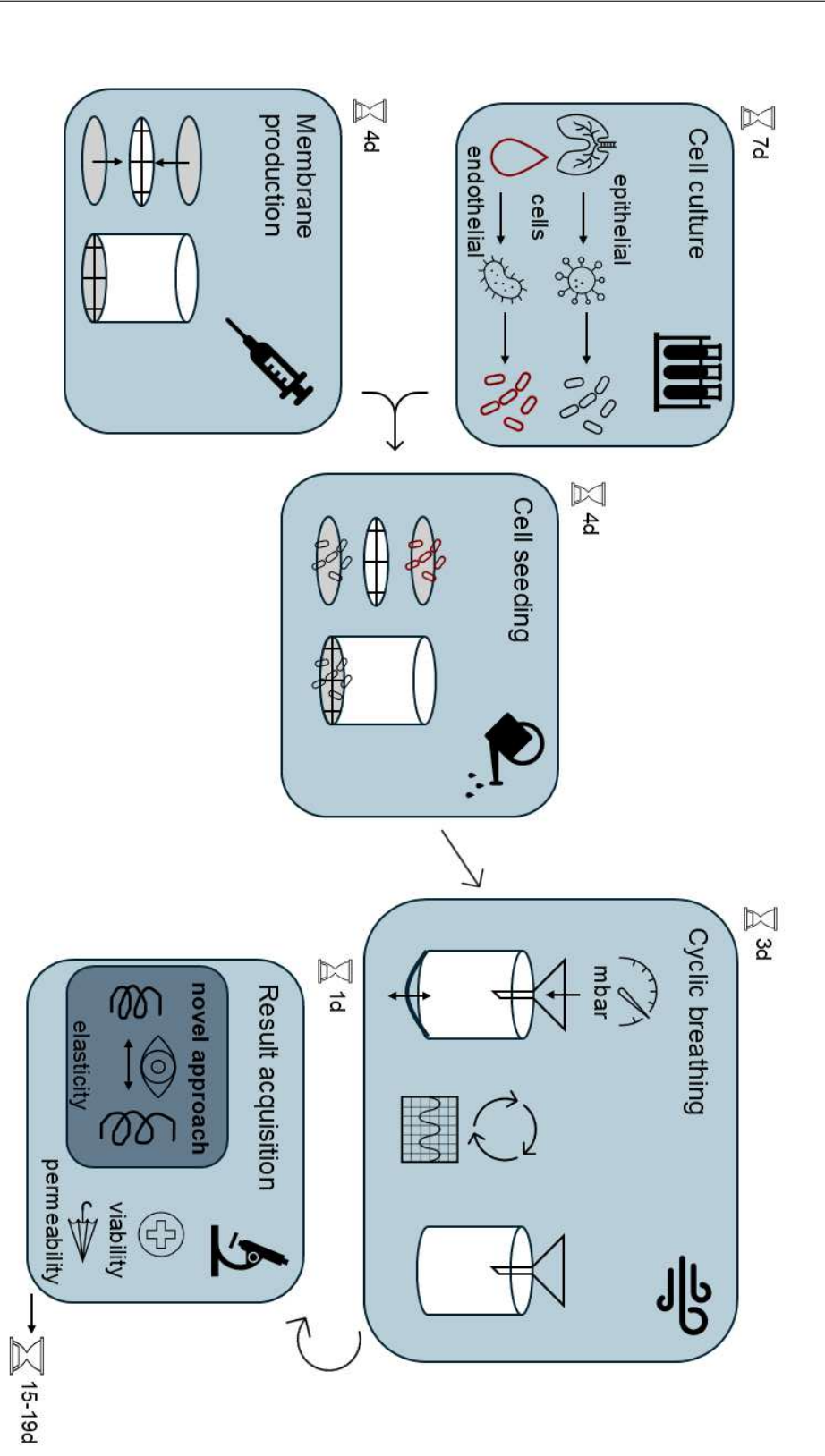


Figure 1.4: Schematic overview of experiment set-up and schedule

Materials and Methods

2.1 **Production of Biological Membrane**

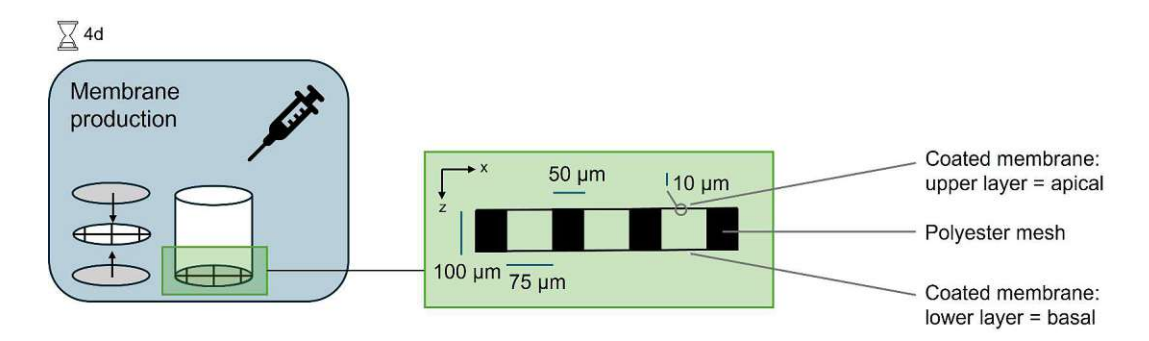


Figure 2.1: Schematic overview: Biological membrane

The CE membrane is produced by pipetting 230 mg of a 1:1 collagen and elastin solution with a concentration of 3.5 mg mL^{-1} onto a polyester-based mesh, embedded in a well. After drying and an intermediate washing step to clear salts (day 2) the mesh is coated from the other side (day 3) and washed again (day 4). The according protocol (ref. A.1) was adapted by [23]. The amount of solution fits the solution-to-area ratio used by the role-model project [3] leading to a similar thickness of the membrane in the range of about 10 µm. In contrast, the double-sided coating (fig. 2.2) ensures the proper attachment of cells, resulting in an overall thickness of about 100 μm, compare fig.2.1. From now on, the terms coated membrane, biological membrane, double membrane, and membrane are used as synonyms in the context of the thesis.



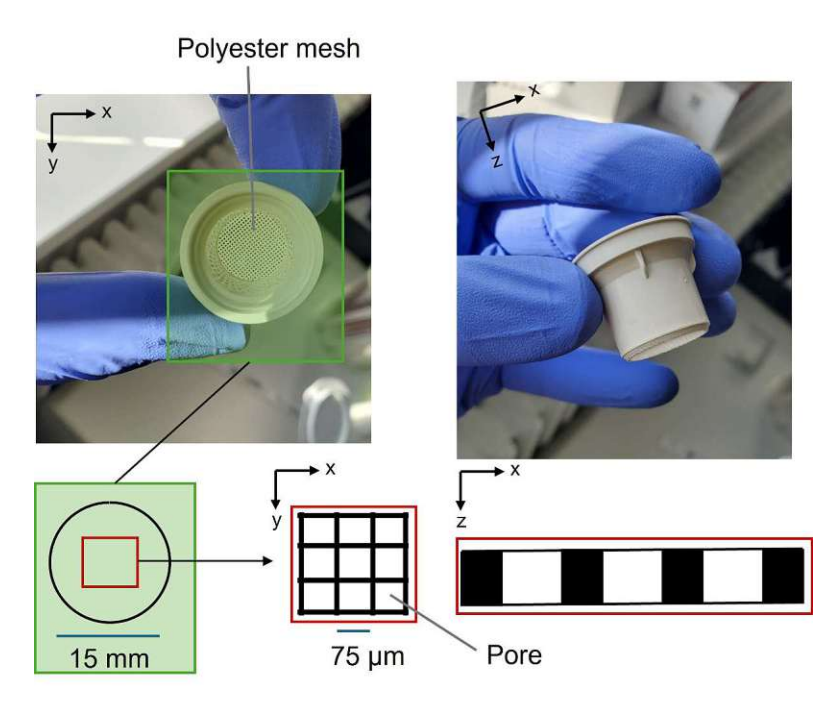


Figure 2.2: Schema of double membrane coated on mesh of well Pictures by Mona Amiratashani (UKJ)

2.2 **Cells**

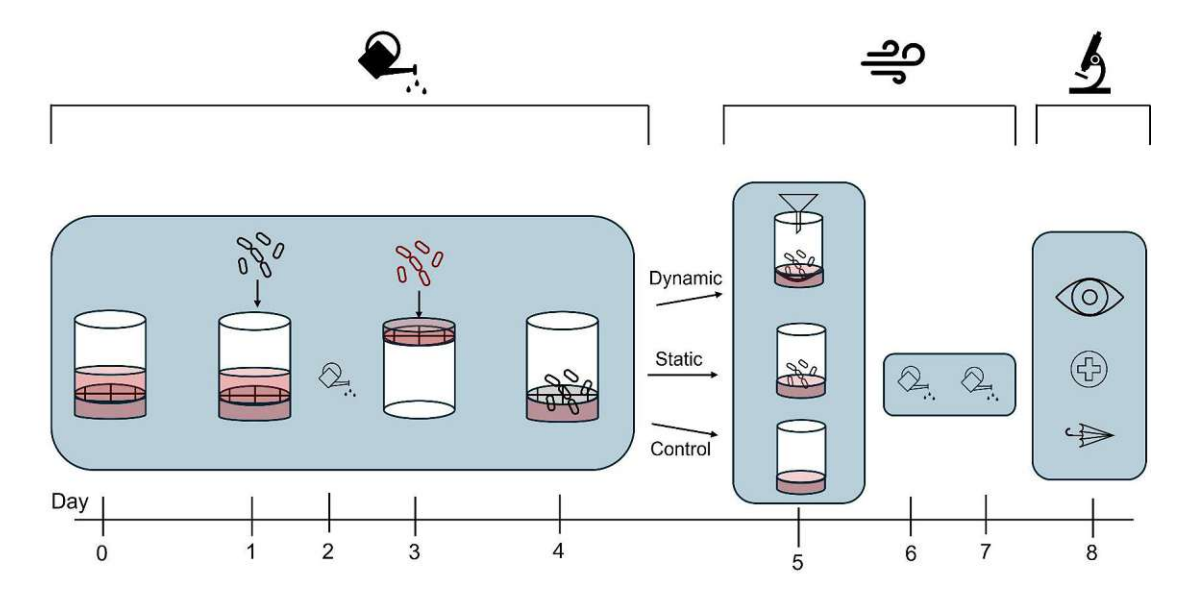


Figure 2.3: Schematic overview: Breathing phase: cells, cyclic breathing, and result acquisition

2.2.1 Cell Culture

The epithelial cells used in this study are *NCI-H441*. Human umbilical vein endothelial cells (HUVECs) are isolated and cultivated by members of our research group in the clinic. The cultivation of both epithelial and endothelial cells follows standardized protocols to ensure reproducibility and viability. Detailed procedures for cell harvesting and culture conditions can be found in the appendix (ref.A.2), the structure of the experiment from the cell seeding to the breathing is represented in fig. 2.3, and the related explanation in A.2.

2.2.2 Cell Seeding

The seeding of cells onto the biological membrane follows a structured timeline to ensure optimal adhesion, differentiation, and physiological mimicry (ref.A.2).

2.3 Cyclic breathing

The wells of the dynamic group are embedded into the chip (Figure 2.4), which serves as the platform for mechanical ventilation. Complete coverage of the bottom side of each well with medium, free of air bubbles, must ensured. A Filter (top right in Figure 2.4) with a pore size of 0.4 µm is attached to the port of the pressure tube, as infection control remains a critical aspect of the overall experimental set-up.

The Breathing system is then activated. Pressure functionality is confirmed by observing the movement of air bubbles under the light microscope. Afterwards, the chip is placed into the incubator. The distance between the transparent bottom of the chip and the base of the well is approximately 2 mm, a critical parameter for subsequent OCT imaging.

The maximum pressure is applied at which the cells remain viable, while still fitting within the physiological pressure range of 1–13 mmHg (translatable to the millibar scale) [20]. Experimental parameters to be set include:

- Duration: Number of days under cyclic breathing.
- **Pressure:** Applied pressure to the chip [mbar].
- **Periodicity:** Breathing rate (BPM); [min⁻¹], following a sinusoidal pattern.
- Filter usage: Ensuring sterile conditions without contamination.

The breathing set-up allows parallel operation of up to four chips. During the breathing phase, the medium is exchanged daily for all groups, including the static and control groups.

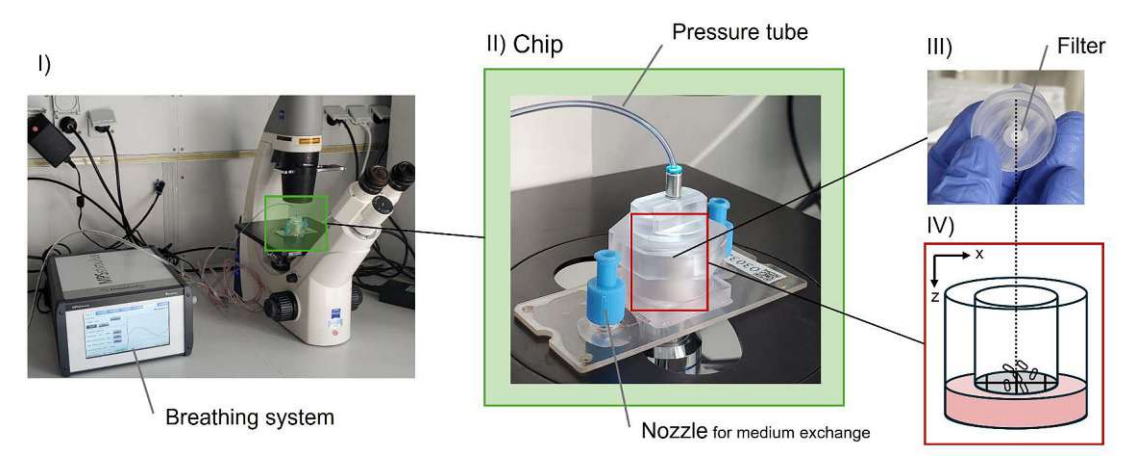


Figure 2.4: Set-up of chip for breathing
Pictures by Mona Amiratashani (UKJ)

2.4 Result Acquisition

At the end of the experiment, the breathing phase is terminated by disconnecting the system and halting pressure oscillation. As elasticity is assessed via OCT, this measurement is conducted first. Subsequent analyses focus on functional assays. A visual inspection is performed immediately after the breathing phase to identify wells that are no longer suitable for further evaluation (detached membranes are readily discernible by eye and excluded from downstream analysis).

2.4.1 OCT

Technique

Optical Coherence Tomography (OCT) is a non-invasive imaging technology based on interferometry with coherent light. By measuring the time delay differences of light beams reflected from different depths within a sample, OCT enables high-resolution visualization of internal tissue structures. A key advantage of this method is its ability to provide real-time depth information without requiring physical contact with the sample. This makes OCT particularly valuable for medical applications.

Spectral-Domain Optical Coherence Tomography (SD-OCT) is an advanced version of this technology that utilizes spectral decomposition of the interference signal. Unlike Time-Domain OCT, which mechanically scans the reference arm, SD-OCT captures the entire depth profile

in a single exposure by employing a spectrometer and a broadband light source. This results in significantly faster image acquisition and improved sensitivity, making it well-suited for dynamic biological imaging. In frequency-domain OCT (FD-OCT), the light source is instantaneously monochromatic, but its wavelength is swept rapidly in time across a range that is similar to that used in SD-OCT. See fig. 2.5

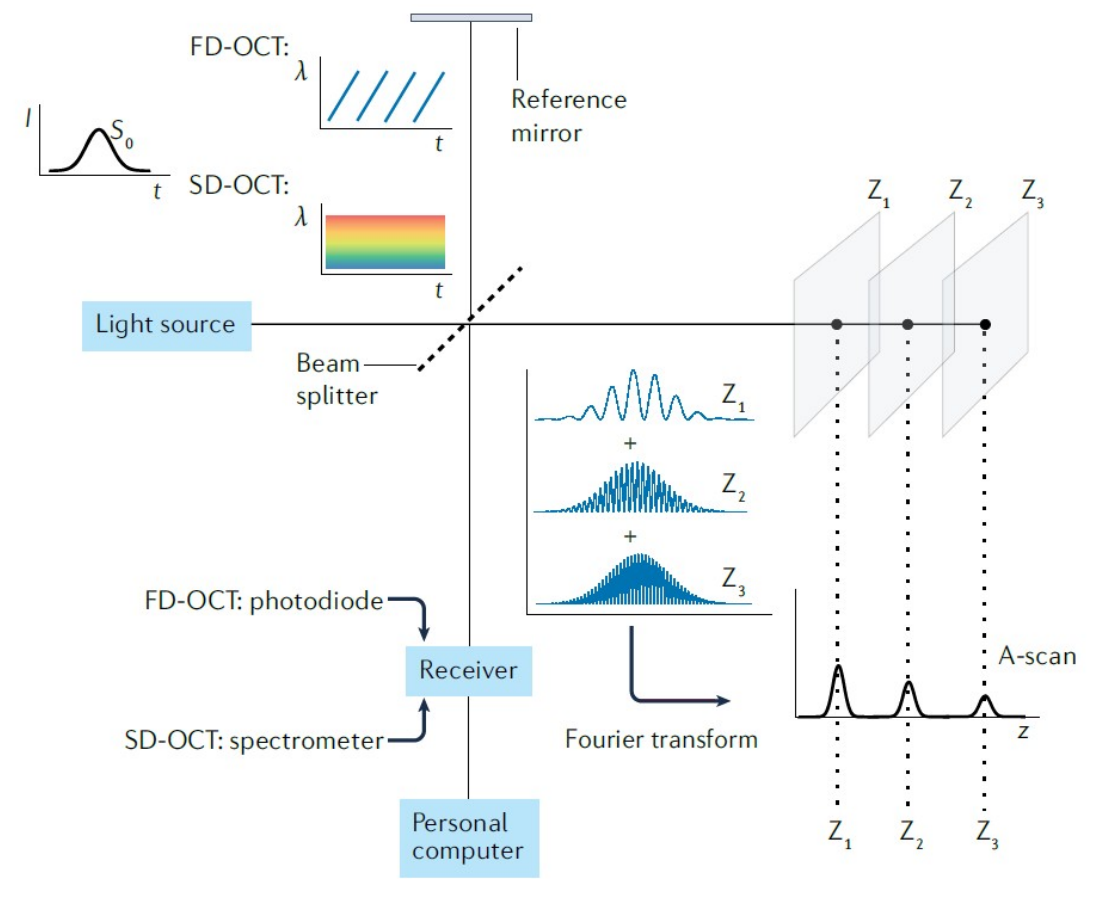


Figure 2.5: Principle of OCT

The resolution of an SD-OCT system is characterized by both lateral and axial parameters. The lateral resolution is primarily determined by the numerical aperture (NA) of the objective lens, with higher NA values leading to improved lateral precision. The axial resolution, on the other hand, depends on the coherence length of the light source and is enhanced by using a broad spectral bandwidth [21]. In this study, the employed SD-OCT system operates with a central wavelength of 750 μ m, an axial resolution of approximately 1.2 μ m in air and a lateral resolution of < 2 μ m for the NIR 1 20x lens. The measurement depth in air is > 700 μ m. More details in A.4.

¹Near-infrared

Protocol

Because the OCT protocol was developed in the course of the experiments and its documentation provides an important basis of knowledge for further experiments, it is listed here and not in the appendix.

- Preparatory phase: Coating of membranes, cell seeding, and initiation of the breathing phase.
- Place heat-retaining packs in the incubator one night prior to the end of the breathing phase.
- At the end of the breathing phase: Disconnect the chips from the breathing system. Transfer the chips (Dynamic group) together with the wells from the Static and Control groups into a Styrofoam box with pre-warmed heat-retaining packs and seal it.
- Transport both the sample box and the breathing system to the OCT workstation².
- Assemble the measurement platform on-site and connect all necessary tubing.
- Detach the filter from the chip. This is essential because accurate strain calculations require
 true pressure values, and the filter may be blocked by residual fluid due to the upside-down
 orientation required by the device set-up.
- Shortly before the measurement, remove excess medium using a syringe:
 - Too wet: causes image noise due to additional reflection lines.
 - Too dry: leads to membrane stiffening, which artificially increases the measured elastic modulus.
- Connect the chip to the pressure source and place it in the test stand.
- Adjust the chip's position (see fig. 2.6 III).
- Align the angle to ensure the biological membrane is in focus rather than the polyester mesh (see fig. 2.6 II).
- Adjust the optical focus.
- Conduct the measurement of the current well.



²Open OCT Lab at Ernst-Abbe-Hochschule Jena(EAH)

TU Sibliothek, Week Your knowledge hub

- Place the mesh on the platform (maintaining sterility as far as possible) and proceed to the next sample. Use the same chip for all wells to minimize chip-related variability, which significantly affects outcomes during the breathing phase:
 - The pressure inlet of the chip is not always centred over the well by manufacturing, resulting in off-centre pressure application.
 - The chip lid may fit loosely onto the core, requiring fixation to ensure sealing.
- After the final measurement: Dismantle the test set-up and return the materials to the lab for subsequent functional assays.

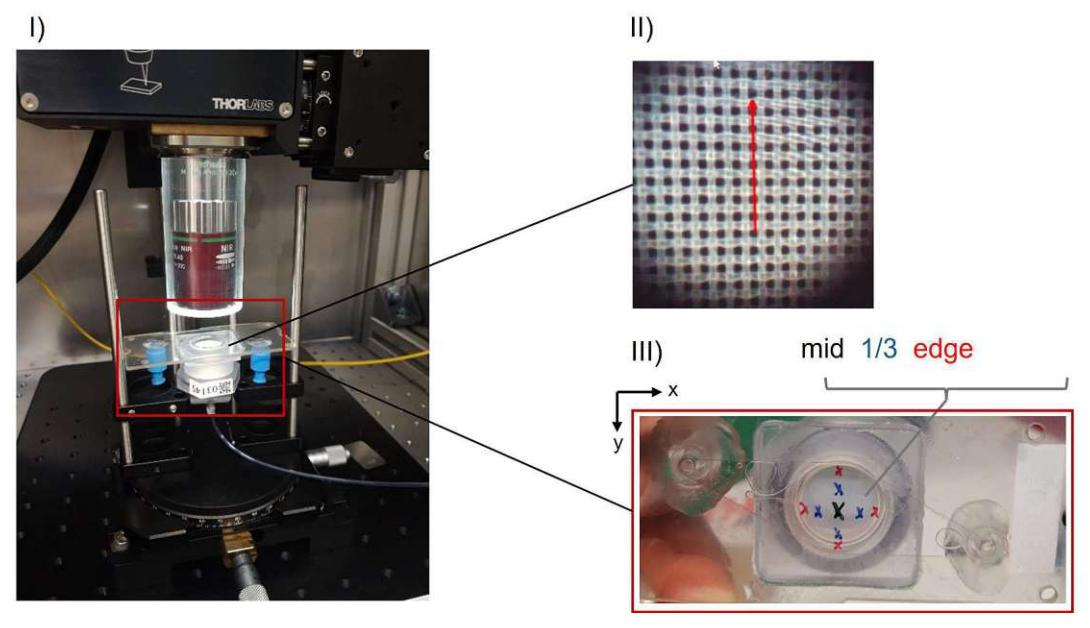


Figure 2.6: OCT protocol: I) Chip in measuring position, upside down. II) Alignment of mesh. III) Positioning within mesh.

2.4.2 Mechanical Assumptions

Having described OCT, an image is used to guide from the Definitions 1.2 to the questions and their answers:

- How can the linear strain value in the membrane be estimated? (Derivation of the Formula for Strain Calculation)
- Is it possible to estimate stress values out of the orthogonally applied pressure? (From Pressure to Stress)

Derivation of the Formula for Strain Calculation

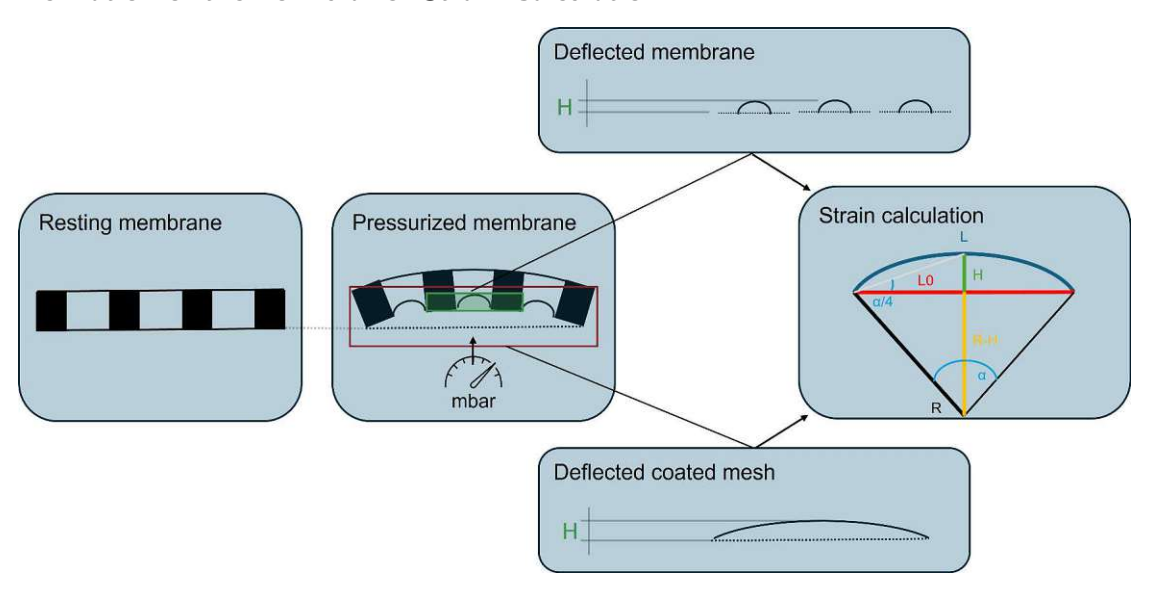


Figure 2.7: Derivation of the Formula for Strain Calculation

While the mathematical formula to predict linear strain on a thin surface based solely on geometric deformation is applied in previous studies [3, 22], its derivation is not explicitly presented. A reconciliation of the approach is provided below, as illustrated in Figure 2.7.

$$R^2 = \left(\frac{L0}{2}\right)^2 + (R - H)^2 \tag{2.1}$$

Expanding the equation using the binomial formula:

$$R^2 = \frac{L0^2}{4} + R^2 - 2RH + H^2 \tag{2.2}$$

to:

$$R = \frac{4H^2 + L0^2}{8H} \tag{2.3}$$

Angles whose legs are perpendicular to each other are equal if the vertices lie outside the angle spaces of the other angle. This means that the triangle from the dashed blue line to the centre line R-H with the enclosing angle alpha / 4 is related to the angle drawn between the red and white line:

$$\alpha = 4 \cdot \arctan\left(\frac{2H}{L_0}\right) \tag{2.4}$$

The arc length L is given by the standard formula:

$$L = R \cdot \alpha \tag{2.5}$$

Getting to the final equation:

$$L = \frac{(4H^2 + L_0^2)}{2H} \cdot \arctan\left(\frac{2H}{L_0}\right) \tag{2.6}$$

This final equation expresses the arc length L in terms of the measurable parameters H and L_0 .

From Pressure to Stress

Seen in a very similar application [24], the bulge test method was applied to transfer the orthogonal pressure to a tangential stress, which acts in the direction of measured strain and may guide us, therefore, to the Young's modulus finally [25].

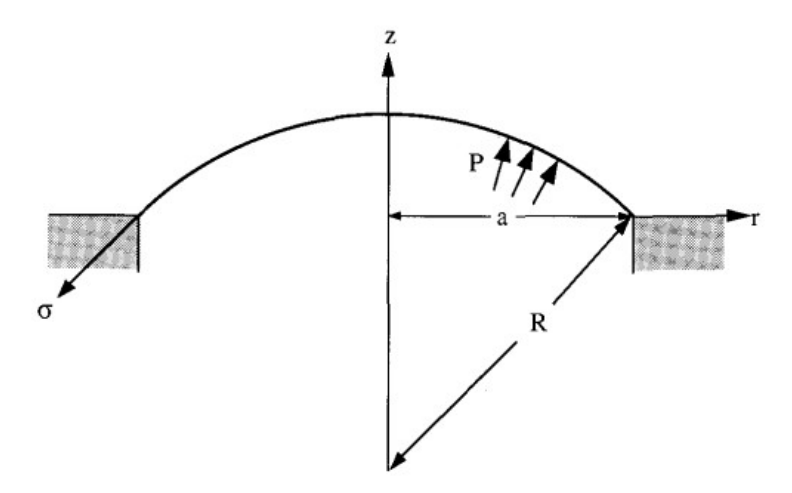


Figure 2.8: Spherical cap geometry used to calculate stress and strain in the bulge test [26]

Starting in [26] from a thin-walled spherical pressure vessel, to the assumption that h is much smaller than a, to

$$\sigma = \frac{Pa^2}{4ht} \tag{2.7}$$

where P is the applied pressure [Pa], a is the characteristic length [m], h is the height of the structure [m], and t is the thickness of the material [m], see fig. 2.8.

3ibliotheky WIEN Your knowledge hub

Data Processing

General OCT Processing Based on the knowledge of the principle of OCT, fig. 2.9 shows the path from the signal to the processed picture (2D) or volume (3D). An A-line (A-scan) is a sequence of pixel values representing a geometric line within a sample, capturing depth-resolved reflectance information. Multiple A-line scans are recorded as the OCT beam moves laterally across the sample. By assembling these A-lines and mapping the reflectance data to greyscale, cross-sectional images (B-scans) are generated, typically maintaining an isotropic scale. When B-scans are collected along a second transverse direction (x-y), they form a volumetric dataset. This dataset can be further processed to extract horizontal cross-sections or en face projections. In some cases, 3D visualization aids in interpretation and facilitates the selection of relevant sub-volumes. For this study, B-scans were generated.

File Conversion The output data of the OCT system was pre-processed with software at the EAH, the acquired data is divided in:

- OCT sequence TIFF file: A multi-frame TIFF file containing optical coherence tomography (OCT) images recorded during mechanical ventilation.
- Camera image TIFF file: A separate TIFF file capturing an image of the sample grid for additional reference.
- **Metadata file:** A text file containing experimental parameters such as study name, scan properties, and pixel size.

To use the data and finally evaluate the strain within the tissue, further processing is required and was fulfilled by the developed code, ref. to appendix A.5.

2.4.3 Processing Steps

The implemented script performs the following operations:

- Conversion of camera TIFF files: The script converts "OCT-Tiff-Camera" files to PNG format while maintaining their folder structure
- **Reduction of time-series images:** To optimize memory usage, OCT image stacks are reduced to a maximum of 150 frames
- Calculation of centre of mass: The vertical centre of mass of structures in the image series is computed based on pixel intensities to analyze movement over time.

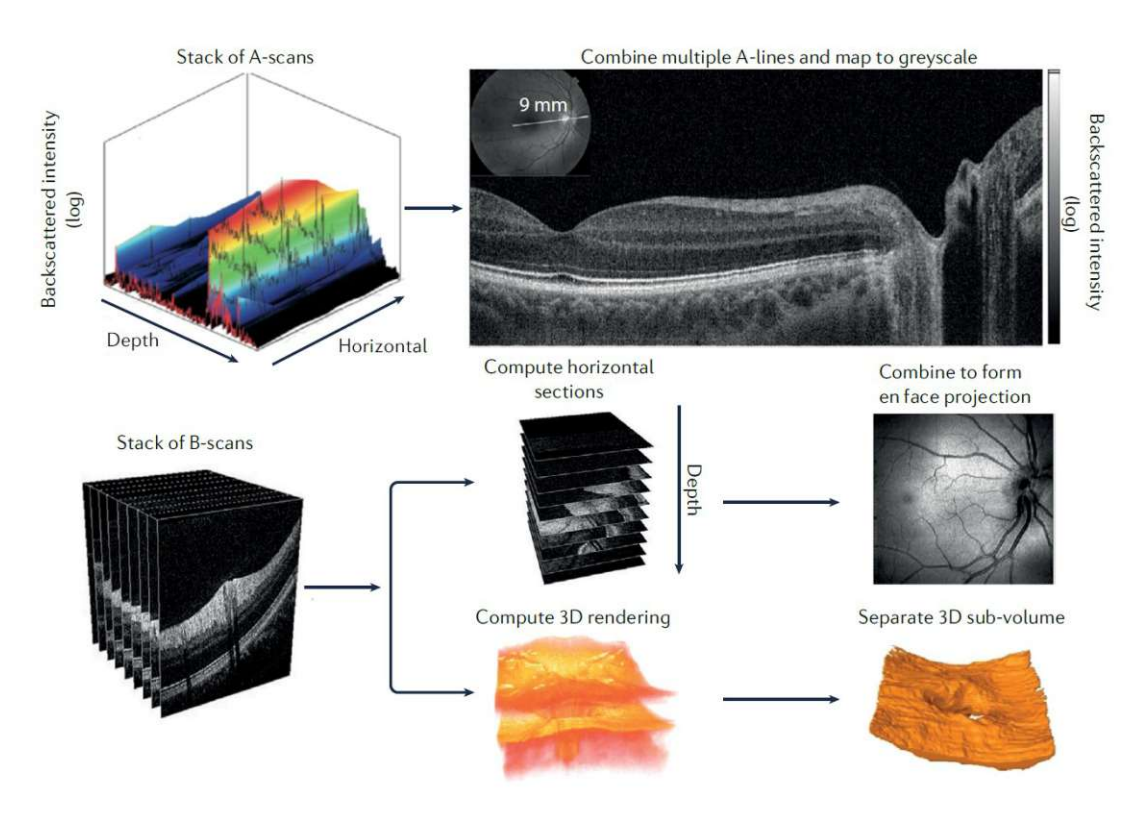


Figure 2.9: Pathway of Processing OCT data [21]

- **Detection of extreme frames:** The frames corresponding to the highest and lowest vertical positions of structures in the time series are identified.
- Scale bar addition: A scale bar is inserted into images using the pixel size extracted from metadata, ensuring accurate dimensional reference.
- Metadata extraction and update: The script reads metadata files, extracts parameters such as study name and scan settings, and updates them with computed pixel sizes.
- File renaming and structured output: Processed files are renamed according to a standardized format, incorporating unique numbering and scan-specific identifiers.
- Storage of extreme frames: The detected extreme frames are saved as PNG images with structured naming for further analysis.



TU Sibliothek, Wilen Your knowledge hub

2.4.4 Permeability

Technique

Fluoresceinisothiocyanat (FITC) is used for permeability assays due to its fluorescent properties [3]. The permeability of the artificial lung barrier is analysed using a small molecule FITC-sodium sized 0.4 kDa ³ and capitalizing on its diffusion capacity.

Protocol

This experimental approach rather compares differences between cell (Dynamic/Static) and non-cell (Control) samples to evaluate the intactness of the cell membranes instead of absolute values. After washing three times by Phosphate-buffered saline (PBS) -/-, the lower chamber (basal = endothelial) is filled with 200 µL of PBS -/-, while the upper chamber (apical = epithelial) is filled equally but with a solution of 1 mg mL⁻¹ FITC-sodium. 50 µL of the solution from the lower chamber is collected after 30 minutes and another 30 minutes. It is analysed using a multi-well plate reader (*M1000 Infinite, Tecan*). Excitation and emission wavelength is set to 460/515 nm. Following a dilution series, the concentration values of the basal side are normalized, see fig. 2.10.

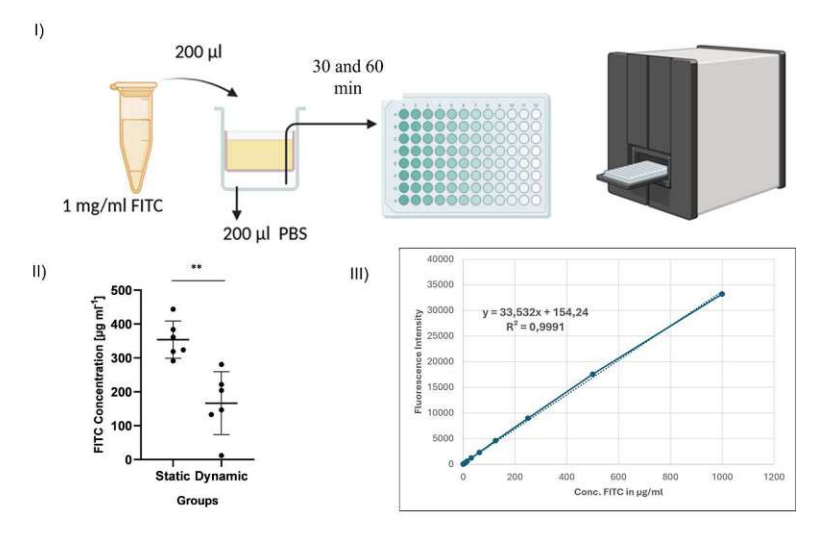


Figure 2.10: FITC-method as viability assay: I) FITC protocol from dilution to results. II) FITC data analysed. III) Calibration curve for analysis.

³Molecular mass of 0.4 kDa is a low-molecular-weight fluorescent tracer commonly used to evaluate membrane permeability. Due to its small size, it readily diffuses across both para cellular and trans-cellular pathways, making it highly sensitive to subtle changes in barrier integrity

A calibration curve is used for every trial to convert fluorescence intensity into concentration values. The equation derived from the dilution series is e.g.:

$$C = 30x + 150 \tag{2.8}$$

where x represents the concentration $[\mu g/mL]$ and C is the fluorescence intensity.

Example for a measured fluorescence intensity of $x = 10^4$:

$$C = \frac{10^4 - 150}{30} = 328,33 \mu \text{g/ml}$$
 (2.9)

Furthermore, the permeability coefficient (P) can be calculated using the following equation and requiring the total transported drug amount (Q) to be known [27]:

$$P = \frac{dQ}{dt} \times \frac{1}{AC_0} \tag{2.10}$$

where:

- dQ is the amount of FITC transported [µg],
- dt = 3600 is the duration of measurement [s],
- A = 1.76 is the membrane surface area [cm²],
- $C_0 = 1000$ is the initial FITC concentration [µg/mL].

Since 50 µL is removed after 30 minutes, the remaining volume for the second sample is $V = 200 - 50 = 150 \mu$ L, altering the concentration due to dilution effects. This reduction in volume can increase the concentration of the subsequently collected sample due to the influx of a more concentrated solution from the epithelial side.

2.4.5 **Viability**

Technique

The Viability Assay includes fluorescence staining and follow-up visualization by Confocal Laser Scanning Microscopy (CLSM).

CLSM is an advanced imaging technique that allows for high-resolution visualization of biological samples by selectively capturing light from specific focal planes. Unlike conventional wide-field

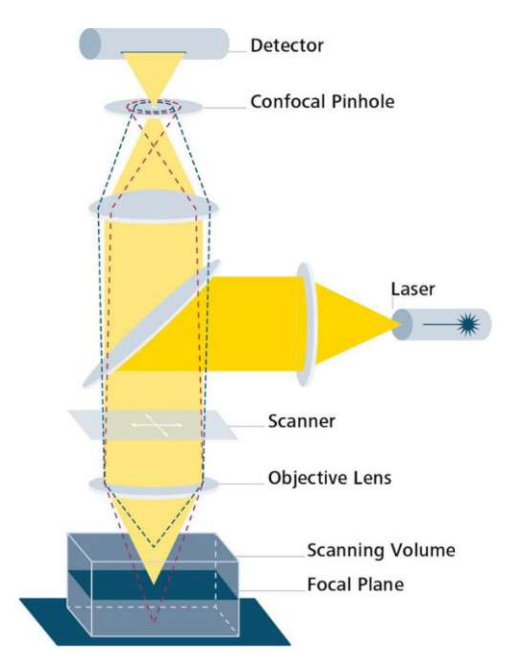


Figure 2.11: Principle of Confocal Laser Scanning Microscopy [28]

microscopy, which collects light from all depths of the sample, CLSM employs a pinhole to block out-of-focus light, significantly improving optical sectioning and contrast.

The system works by scanning a focused laser beam across the sample, exciting fluorescent molecules at defined wavelengths. The emitted fluorescence is then detected through a pinhole aperture, ensuring that only light from the focal plane of interest is collected. By sequentially acquiring multiple thin optical sections at different depths (a process known as z-stacking), CLSM enables the reconstruction of detailed three-dimensional (3D) images of the sample.

CLSM allows for high-resolution imaging of biological samples by selectively exciting fluorescent markers. In a viability assay, different fluorescent dyes are used to distinguish between live and dead cells, as well as to stain specific cellular structures. The *LSM 900, ZEISS* is used in this study.

The following fluorescent markers were used for the viability assay [29]:

Reagent	Function	Concentration (per 10 ml)
Hoechst 33342	Nuclear stain (all cells, blue fluorescence)	1:1000 (10 µl)
Ethidium Homodimer-1	Stains dead cells (red fluorescence)	20 μl
Calcein-AM	Stains viable cells (green fluorescence)	5 μl

Table 2.1: Fluorescent reagents used for cell viability staining.

Protocol

- Thaw Ethidium Homodimer-1 and Calcein-AM, vortex briefly to ensure homogeneity.
- Prepare staining solution in PBS $^{+/+}$ by mixing reagents according to Table 2.1.
- Place cell-seeded wells in a 6-well plate, prefilled with 400 μ l PBS $^{+/+}$ in both apical (top) and basal (bottom) compartments. Aspirate PBS before staining.
- Add 350 µl of the staining solution to both the apical and basal compartments.
- Incubate samples for 30 minutes at 37°C in a humidified incubator, protected from light.
- \bullet Carefully aspirate the staining solution and wash cells with 500 μl PBS $^{+/+}$ (apical and basal).
- Keep samples light-protected (e.g., wrapped in aluminium foil) and proceed immediately to CLSM.

This staining protocol enables a clear distinction between viable and non-viable cells while providing structural information about cell adhesion, which is crucial for analysing cell viability in tissue culture experiments.



CHAPTER

Results

3.1 **Trials**

	Trial	Date	Objectives		Methods	;
				OCT	Perm.	Viab.
	1	07.05.	Introduction to membrane production and			
			cell culturing			
ests	2	22.05.	First guided trial with cells		✓	\checkmark
Pre-tests	3	30.05.	Second guided trial with cells		✓	\checkmark
Pr	4	11.06./12.06.	First OCT tests	✓		
	5	31.07.	Second OCT tests	✓		
	6	12.08.	Test of different coatings (pore sizes, single /	✓		
			double) and filters			
	7	30.09.	OCT system not accessible		✓	\checkmark
Est	tablish l	biological* and	OCT site:			
	8	24.10.	2× dynamic, 2× static, 1× control	✓	✓	√
Main	9	30.10.	2× dynamic, HUVECs dynamic**, H441 dy-	✓	✓	
Ž			namic, 3× static, 1× control			
	10	25.11.	2× dynamic, 1× static, HUVECs dyn/stat,		✓	\checkmark
			H441 dyn/stat, 1× control			
	11	02.12.	$3 \times$ dynamic, $3 \times$ static, $3 \times$ control	✓		

Table 3.1: Overview of experimental trials and methods of analysis

Perm. = Permeability, **Viab.** = Viability



^{*} Conditions of membrane, duration and parameters of breathing

^{**} HUVECs / H441: Only one cell type seeded on the respective side

The experimental results are presented in a structured and representative manner. For clarity, they are organised according to the respective methods. Depending on the planned start of cell seeding onto the biological membranes, and the availability of the OCT set-up, the thawing of new cells or the splitting of confluent cell layers must be carefully coordinated. While the introduction outlines an approximate 15–19 day cycle for the complete set of experiments (see Figure 1.4), the shorter timelines of individual steps necessitate a partial overlap of experimental phases. This overlap presents both advantages and risks: on the one hand, a failure in one phase (e.g., unsuccessful membrane coating) would result in the loss of preparation efforts for subsequent phases. On the other hand, avoiding overlaps would considerably extend the already time-intensive workflow.

3.2 OCT

3.2.1 General remarks

Experiment 4 served as an initial trial of the OCT technique, starting with the first captured image:

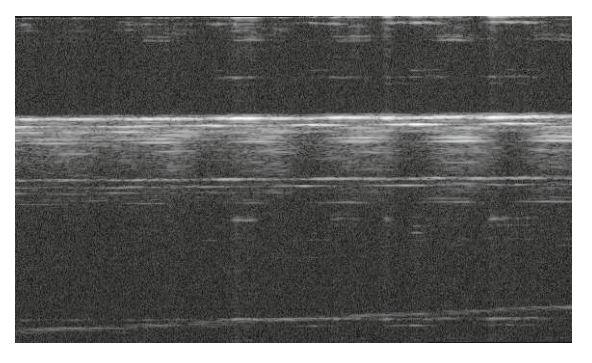
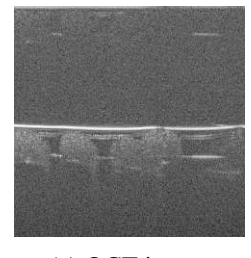
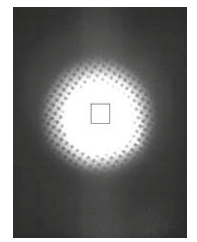


Figure 3.1: First OCT capture

Subsequently, the positioning was refined to a non-planar orientation:



(a) OCT image



(b) OCT camera view

Figure 3.2: Trial 4: OCT cross-section and external OCT camera image

TU Sibliothek, WIEN Your knowledge hub

This was followed by the acquisition of the first usable image of the coated membrane under dynamic loading:

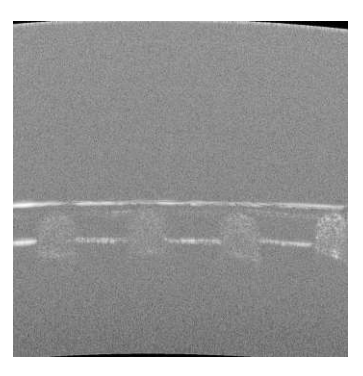


Figure 3.3: Deflection image of the coated membrane during dynamic loading (Trial 4)

By referencing the technique for detecting the deflection of both the membrane-coated mesh and the isolated biological membrane, as illustrated in Figure 2.7, the procedural loop is completed:

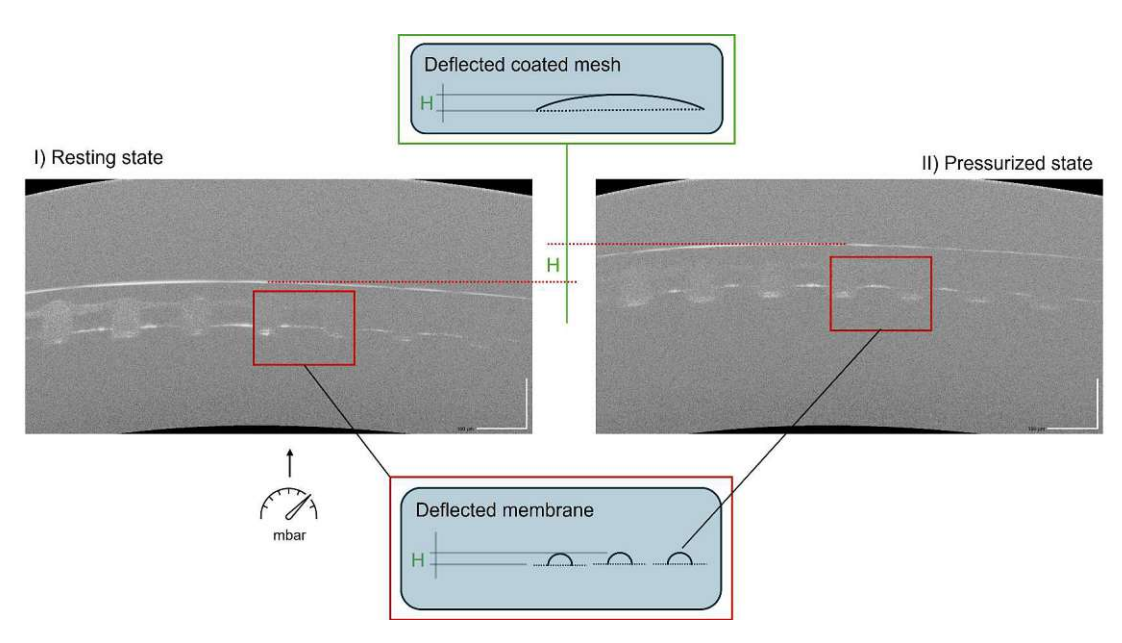


Figure 3.4: Deflection measurement of the biological membrane

Both resting and pressurised states represent the extreme positions during the cyclic breathing motion and are therefore essential to capture. In the following tables, these states are referred to as *up* and *down*. Averaging of images did not lead to an observable improvement in image quality.

IV Sibliothek, Die a wien Your knowledge hub

It should be noted that successive B-scans are not necessarily recorded in equidistant time intervals, precluding the generation of live video footage. This limitation results from the intensive computational demands of OCT imaging.

All scale bars are set to 100 µm.

The following subjectives can be studied:

- Deflection of the membrane-coated mesh
- Deflection of only the biological membrane

Data Processing As discussed in 2.4.2, the original *TIFF* files are approximately 1 GB each, presenting a significant data handling challenge. The conversion to compressed images, as implemented by the code provided in the appendix (A.5), reduced the overall data volume of the OCT main tests from 328 GB to 1.6 GB. Subsequent reduction steps decreased the number of images from 460 to 196 (A3), and a further format conversion from PNG to JPG resulted in a final size reduction from 640 MB to 64 MB.

Additionally, the high input of image files, increased the pdf-version of the thesis to more than 300 MB, which needed to be compromised by at least factor 10 at the end of the writing process.

3.2.2 **Pre-tests**

The pre-tests were conducted to evaluate the applicability of OCT for screening membrane structures and, in parallel, to optimise the biological conditions of the membranes. Final biological parameters were established following Trial 7, including the standardised coating procedure (see Section A.1) and the adjustment of breathing parameters (see Section 2.3): Since then, the proper

Parameter	Value	Unit
Duration	3	days
Pressure	6	mbar
Periodicity	20	bpm [min ⁻¹]
Filter	yes	Pore size 0.4 µm

Table 3.2: Parameters breathing

testing could start on the basis of the same conditions. Images referenced are A2. Observations:

- Filter during OCT: ref. deflection of membrane without filter (9/10) vs. filter 0.4 µm pore size (7/8) and filter 0.2 µm pore size
- Single coating (3/4) at dry conditions
- Reflection of additional water on the sample (5/6)

Filter influence during cyclic breathing

Preliminary experiments indicated that while standard operation with a 0.4 µm filter generally maintained adequate pressure dynamics, occasional blockages by residual liquid could substantially impair pressure transmission. This effect was notably observed during specific pre-tests (A2 11,12), resulting in reduced strain at nominally high pressures (A3, 157/158, 50 mbar). However, across the majority of trials, minimal influence on mechanical loading was assumed under regular filter conditions. During Trial 11, to prevent any potential artefacts during optical coherence tomography (OCT) measurements, the filter was entirely removed.

The double membrane is clearly visible, ref. to fig. 2.1

3.2.3 **Main Tests**

The most important findings are listed on the basis of recordings within a trial (11). Images can be found in the appendix, see A3, also the following embedded with numbers in brackets:

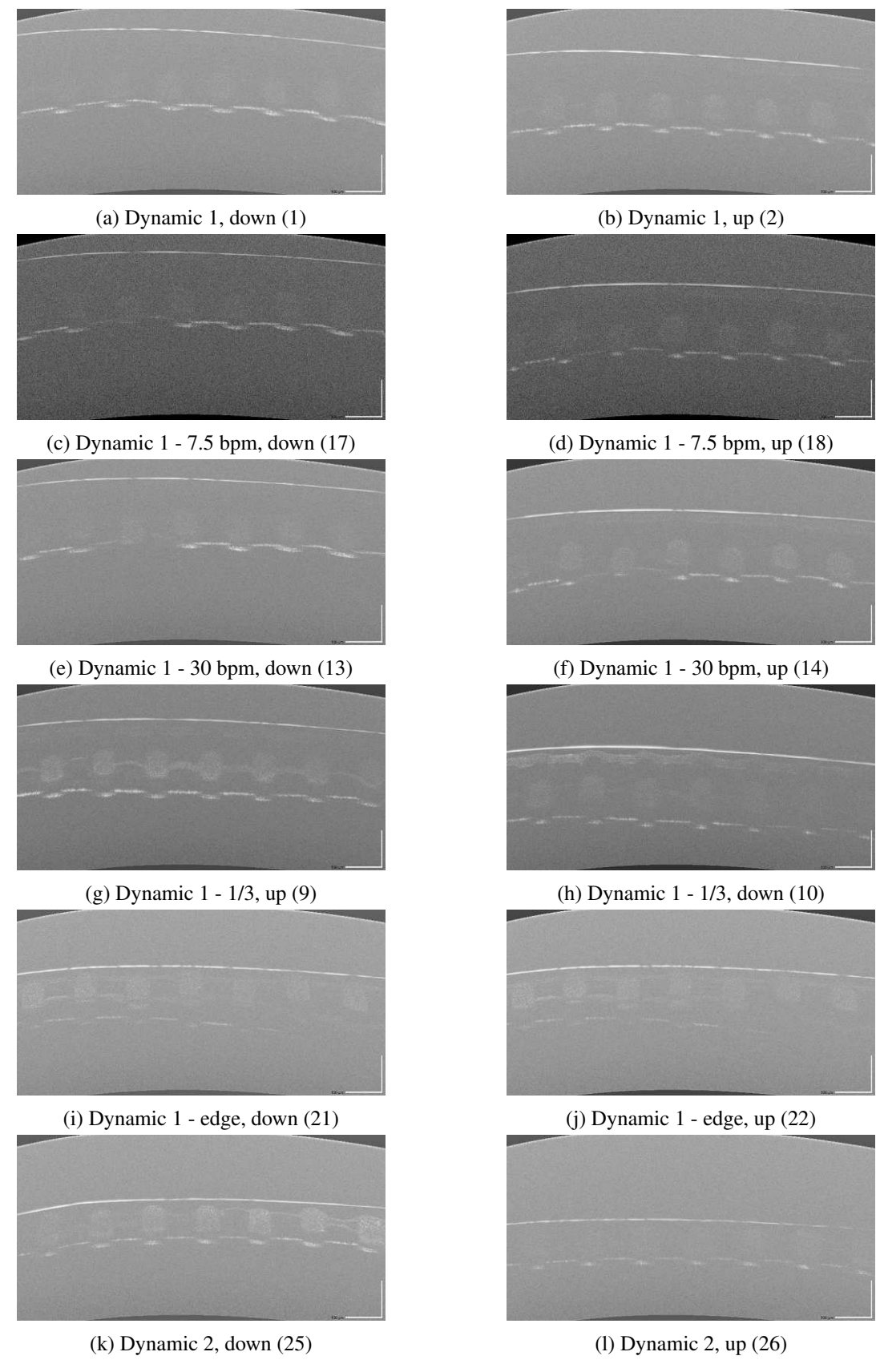


Figure 3.5: Trial 11: OCT images Dynamic

30

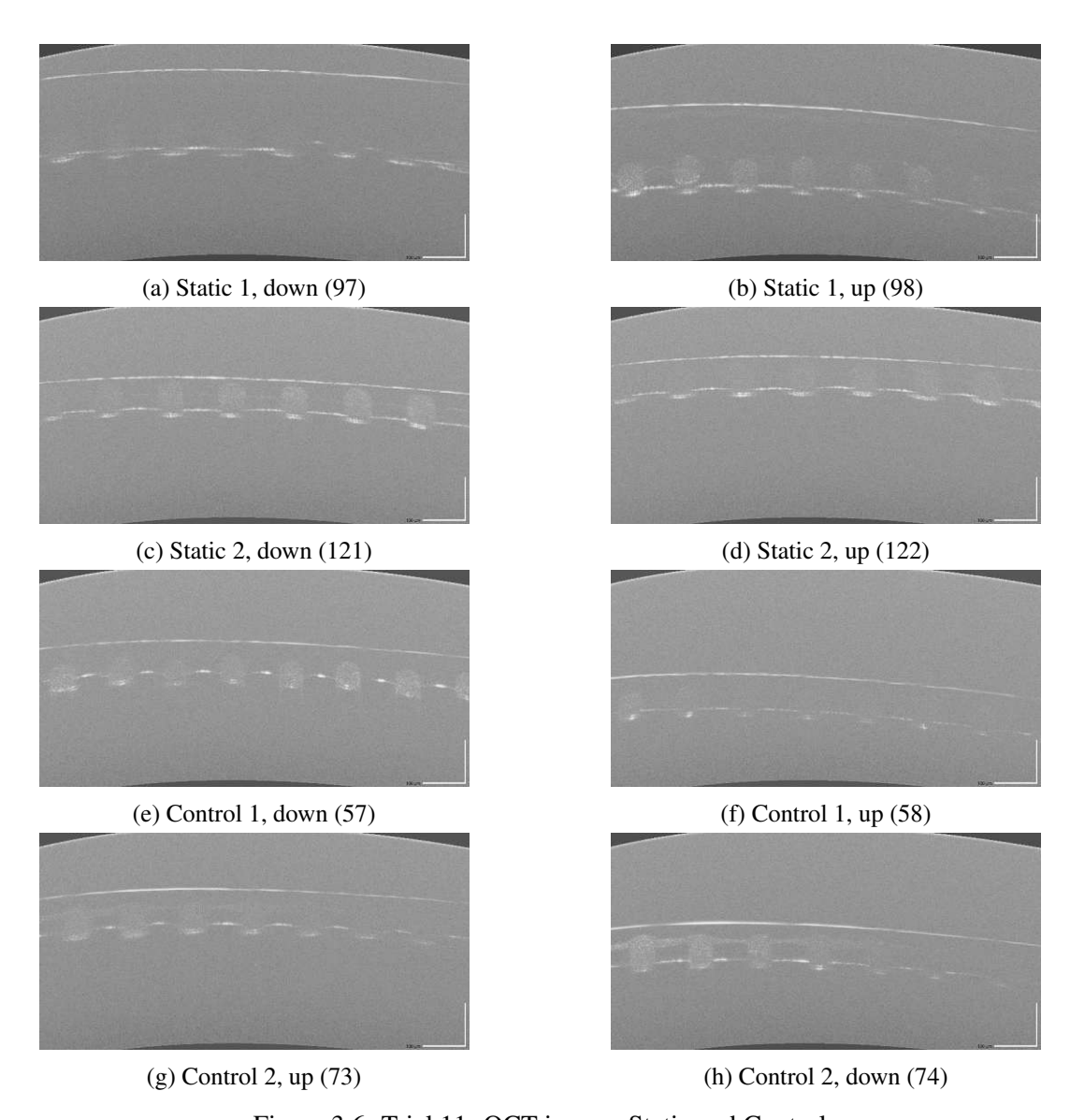


Figure 3.6: Trial 11: OCT images Static and Control

Other observations include heterogeneity as representatively shown:

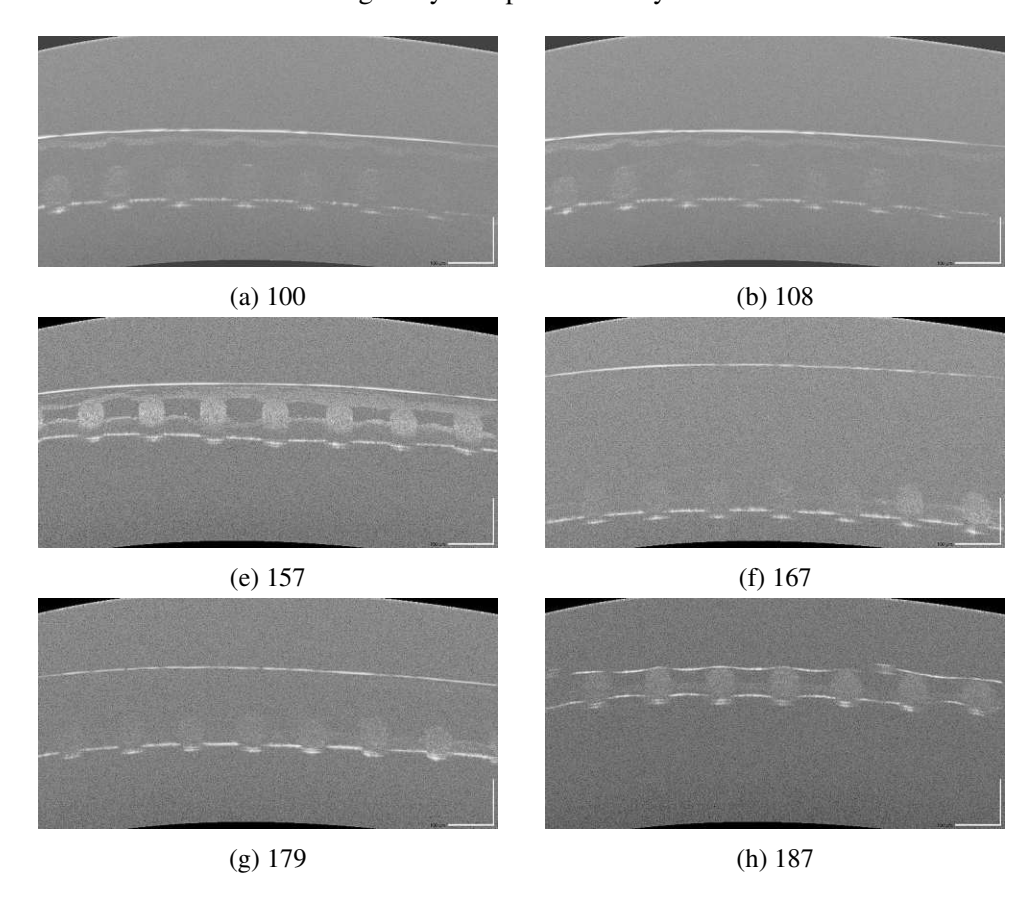


Figure 3.7: Trials 8-11: OCT images Heterogeneity

Deflection of only the Biological Membrane Approximate the linear strain using the following geometric expression, starting from formulae described in section 2.6:

$$L = \frac{(4H^2 + L_0^2)}{2H} \cdot \arctan\left(\frac{2H}{L_0}\right) \tag{3.1}$$

where:

- $L_0 = 75 \,\mu\text{m}$ (initial length)
- H varies from 2 to 30 μm

The strain is then set as:

$$\varepsilon = \frac{L - L_0}{L_0} \tag{3.2}$$

The stress is given by:

$$\sigma = \frac{Pa^2}{4ht} \tag{3.3}$$

- *P* [mbar] (converted to Pa: 1 mbar = 100 Pa)
- $a = 37.5 \, \mu \text{m} = \frac{L_0}{2}$
- H varies from 2 to 30 μm
- $t = 10 \, \mu m$

Pressure [mbar]	<i>Η</i> [μm]	Strain [-]	Strain [%]	Stress [kPa]	$E = \sigma/\varepsilon$ [kPa]
2.5	2	0.002	0.190	4.395	2318.746
5.0	5	0.012	1.181	3.516	297.681
7.5	10	0.047	4.675	2.637	56.397
10.0	20	0.180	17.998	1.758	9.767
15.0	30	0.383	38.322	0.586	1.529

Note: Strain [%] is computed relative to the original length $L_0 = 75 \,\mu\text{m}$.

Assuming a linear elastic behaviour in the lower strain regime (up to \sim 5%), a rough approximation of the Young's modulus can be taken from the ratio at low pressures. For example, between 2.5 and 5 mbar, the modulus ranges from approximately 15 kPa to 50 kPa, suggesting a Young's modulus in the range of:

$$E \approx 20 \,\mathrm{kPa}$$

Deflection of the Membrane-Coated Mesh Given $L_0 = 15 \,\mathrm{mm}$, $H = 70 \,\mathrm{\mu m}^1$, $a = 7.5 \,\mathrm{mm}$, $t = 100 \,\mu\text{m}$ and $P = 10 \,\text{mbar}$ ($P = 1000 \,\text{Pa}$), the membrane experiences approximately 0.58 % strain at a stress of 2.01 MPa, corresponding to an apparent Young's modulus of about 34.6 MPa.

¹Deflection of the membrane-coated mesh occurs mostly in the range of 50 t0 100 μm

In addition to the most important finding followed here, further observations are listed below:

➤ OCT allows live monitoring for biological membranes in the range of millimetres.

For all experiments in which no movement is visible in the cell-seeded membranes, there is a

Observation	Reference	Sample
Physiological strain distribution	a/b	g/h; i/j
(less at edges)	(Results	
	fig.3.5)	
Higher bpm \rightarrow lower elasticity	c/d	a/b; e/f
(dynamic stretch)		
Higher pressure \rightarrow higher strain		A.6
All nets show up/down motion		A.6
reduced with cells		
Elasticity in pores without cells	Control	Dynamic and Static
(acellular) during breathing		
No elasticity in pores with cells	Control	Dynamic and Static
Heterogeneity within samples		-
(If membrane is thicker, then in cell-seeded cases)		

Table 3.3: Summary of observations from mechanical stimulation experiments

control-probe, which, however, shows this movement.

Although a quantitative evaluation could, in principle, provide more detailed insights, it would imply a level of precision that exceeds the actual measurability of the data, thus leading to spurious accuracy. Furthermore, the time and resources required for such an analysis would be disproportionate to the added value of the results, making it neither methodologically justified nor efficient from a time-management perspective. Trends can be approximated:

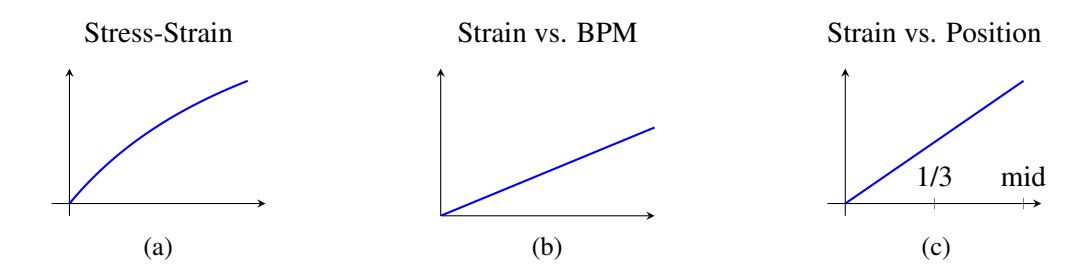


Figure 3.8: Abstracted representation of mechanical trends: (a) stress-strain behaviour, (b) strain as a function of breathing rate, (c) strain distribution across the membrane.

The OCT system used in this study has a depth of focus of approximately $100 \mu m$, which corresponds closely to the thickness of the membrane itself. As a result, the dynamic analysis was limited to the lower membrane interface.

3.3 Permeability

Only **Static** and **Dynamic** conditions were evaluated statistically. Other groups were not included in statistical comparison but follow expected trends. Time and effort involved in the work only allowed for a few samples. Data was evaluated on two levels:

- Across all experiments (regardless of minor experimental condition differences)
- Subset of experiments with identical conditions (n = 3)

Trial	Static 1	Static 2	Dynamic 1	Dynamic 2	Control	Dead	Dyn. H441	Stat. H441	Dyn. HUVECs	Stat. HUVECs
2	319		12							
3	444		281		569	525				
7	324		147							
8	298	285	110	156						
9	399	324	235	174						
10	480	288	222	563			463	388	430	438

Table 3.4: FITC concentration data $[\mu g m L^{-1}]$ across trials and experimental conditions. The yellow value was excluded from analysis due to membrane rupture in the corresponding sample.

Data analysis is conducted using *GraphPad Prism 8* software. Data are presented as mean \pm standard deviation (SD). The error bars represent the SD. Two-tailed unpaired Welch's t test was used to assess the significance of differences. Statistical significance was defined as follows: *p < 0.05, **p < 0.01, ***p < 0.001 and ****p < 0.0001.

3.3.1 Analysis Across All Experiments

To compare the impact of static and dynamic conditions across all experimental data, a two-tailed Welch's *t*-test was applied. This test revealed a statistically significant difference between the *Static* (M = 354.0 µg/ml) and *Dynamic* (M = 166.6 µg/ml) groups, with a mean difference of -187.4 ± 43.98 µg/ml (p = 0.0027). The confidence interval for the difference was [-288.5, -86.24] µg/ml. The calculated effect size ($\eta^2 = 0.6907$) indicates a strong effect, suggesting that dynamic conditions markedly reduce membrane permeability.

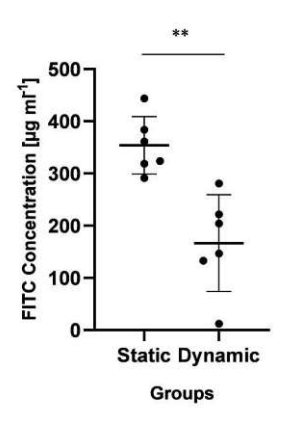


Figure 3.9: Welch's test: Individual values with Mean and SD by groups

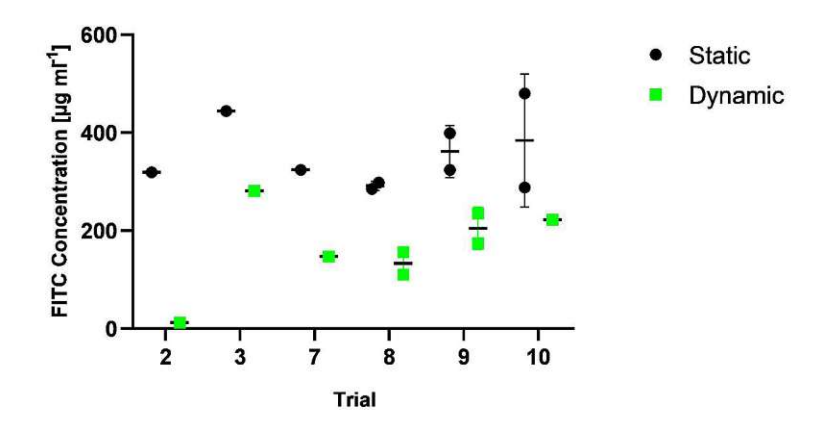


Figure 3.10: Welch's test: Individual values with Mean and SD by trial

Table 3.5: Welch's *t*-test Results

Measure	Static	Dynamic
Mean	354.0	166.6
Difference (B - A)	-187.	4 ± 43.98
95% CI	[-288.	5, -86.24]
<i>p</i> -value	0.00)27 (**)

3.3.2 **Identical Experimental Conditions**

To assess the robustness of this effect under controlled conditions (trials 8,9,10), a linear mixedeffects model was applied to a subset of experiments with identical set-up (n = 3). The model

controlled for the fixed effects of Condition and Experiment, as well as their interaction, to account for systematic differences across trials. Additionally, random effects (e.g., biological replicates) were included to capture within-experiment variability. This approach allows for isolating the impact of dynamic versus static conditions while accounting for inter-experimental heterogeneity.

Table 3.6: Mixed-Effects Model Results (Identical Conditions Only)

Effect	<i>p</i> -value	Significant?	F-value	Interaction?
Condition	0.0903	No	F(1,2) = 9.603	_
Experiment	0.2870	No	F(1.36, 2.05) = 2.248	_
Cond. \times Exp.	0.9975	No	F(2,3) = 0.002	No

Although the *Condition* effect did not reach statistical significance (p = 0.0903), the F-statistic (F(1,2) = 9.603) indicates a trend toward a meaningful difference, consistent with the direction and magnitude observed in the Welch's test.

3.4 Viability

To assess cell viability and vertical distribution within the tissue, ZEN 3.10 (Zen lite) software (ZEISS) was used to analyse z-stacks obtained from confocal imaging. Two types of projections were generated for evaluation:

Orthogonal projections consisted of a stack of images acquired along the same z-axis. These were evaluated based on the highest intensity signal, allowing a qualitative assessment of viability across depth. Colors are reminded as: Calcein for viable cells (green), Ethidium for dead cells (red) and Hoechst for nuclei (blue).

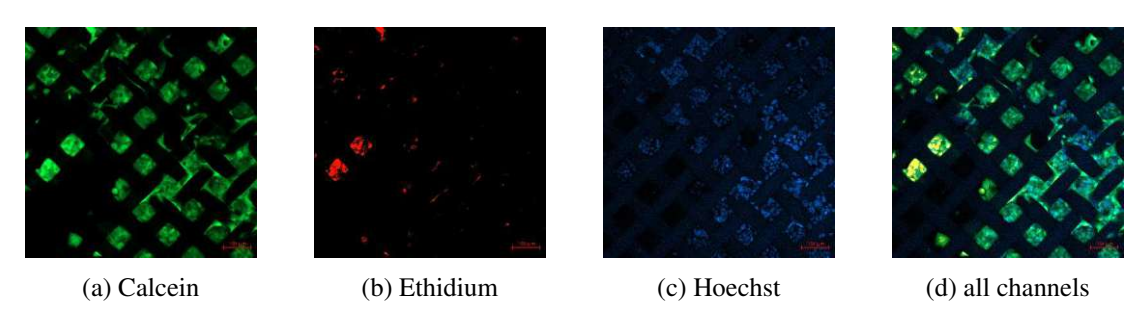


Figure 3.11: Trial 10: Orthogonal projection - Dynamic

Colour-coded projections assigned colour gradients to signal intensities along the z-axis. This enabled positional identification of intensity peaks, thus highlighting where cells were distributed vertically within the tissue. These projections answered the question of spatial cellular distribution (i.e., "Where do cells spread along z?").

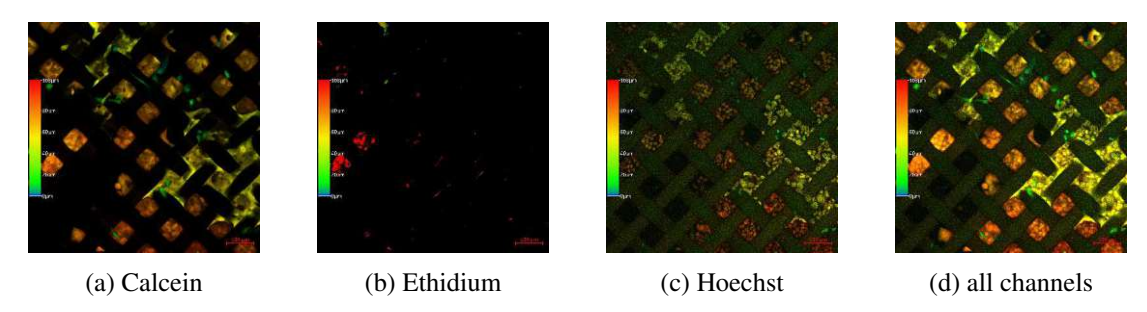


Figure 3.12: Trial 10: Colour-coded projection - Dynamic

Across all experimental group viability analysis demonstrated consistent survival of cells at different positions and depths within the membrane. Orthogonal projections from multiple regions confirmed the presence of intact and viable cells across the entirety of the biological net structure. It needs to be mentioned that on a test basis just some spots were tested randomly, see (fig. 3.13). The main focus is on the fact that the endothelial cells (HUVECs) appear to migrate into the tissue and thus favour stiffening. Images are attached at A.7.

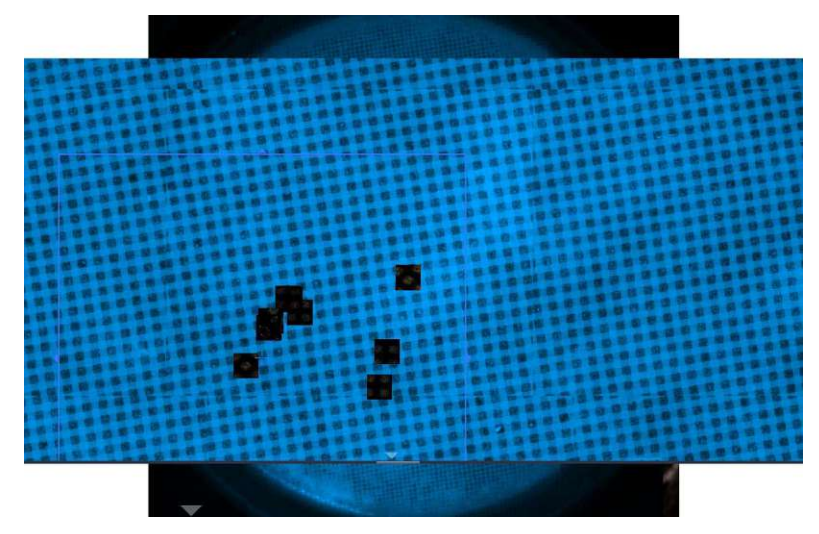


Figure 3.13: Sample overview: Viability assay Pictures by Mona Amiratashani (UKJ)

Discussion

OCT

Box 1: Parameter Trends: Breathing system to Membrane

- **Duration:** (not enough data)
- **Pressure:** increase $\uparrow \rightarrow$ increase in strain \uparrow
- **Periodicity:** higher rate $\uparrow \rightarrow$ decrease in strain \downarrow
- Filter pore size: decrease $\downarrow \rightarrow$ decrease in pressure \downarrow

The parameter analysis (ref. 3.2) revealed that both pressure and frequency of mechanical stimulation play critical roles in defining the resulting strain on the biological membrane. Increased pressure consistently led to greater strain, as expected in a deformable collagen-elastin matrix. In contrast, increasing periodicity (i.e., the breathing frequency) was associated with a reduction in measurable strain. This phenomenon can be attributed to the viscoelastic behaviour of collagen, which responds differently to rapid cyclic loading—exhibiting stress relaxation and internal damping that reduce peak deformation. Additionally, spatial analysis of the membrane confirmed a non-uniform strain distribution, with central areas exposed to the greatest mechanical load. Filter properties, such as pore size, also affected the effective pressure transmitted to the membrane, influencing strain indirectly.

TU Sibliothek, Die approbierte ger WIEN Vour knowledge hub
The approved origi **Note:** Potential pressure losses due to filter resistance were observed in preliminary tests, which may slightly affect strain transmission fidelity.

Box 2: Summary: OCT

- Strain distribution: physiological profile with reduced strain at the edge.
- Elasticity (w/o cells): membrane within pores deforms elastically during breathing, approx. 10% at 10 mbar and 20 bpm in centre region, Young's modulus in the range of kPa.
- Elasticity (w/ cells): no visible deformation in pore membranes under breathing conditions.
- **Membrane-coated mesh motion:** up/down movement observed in all conditions; reduced motion with cells.
- Tissue characteristics: cells may increase local thickness, thus stiffness.
- Breathing frequency: higher bpm \rightarrow lower stretch (elastic response).

The stress calculations applied in this study (section 2.4.2 to 3.2.3) are based on bulge test models originally developed for thin-walled structures with a high aspect ratio, where lateral dimensions significantly exceed thickness. The membranes here do not meet these geometric criteria (figures 2.1, 2.2), therefore, the applicability should be interpreted with caution.

Considerations regarding Collagen Mechanics In addition, it must be considered that the mechanical behaviour of collagen-rich materials is highly sensitive to several structural parameters. For example, hydration plays a dominant role: upon dehydration, the indentation modulus of collagen fibrils increases by up to three orders of magnitude, shifting from approximately 1–15 GPa (dry) to 2–450 MPa (wet) as measured by atomic force microscopy. Furthermore, enzymatic cross-linking and the accumulation of advanced glycation end-products (AGEs) markedly alter collagen fibril stiffness and viscoelastic behaviour, as shown by significant differences in tensile modulus between immature and mature cross-linked fibrils. Future studies incorporating simultaneous structural imaging (e.g., SEM or TEM¹) and mechanical testing may provide more comprehensive insights into the spatial heterogeneity and remodelling of the membrane under cellular influence [30].

¹Scanning -, Transmission electron microscopy

Permeability

To robustly evaluate the influence of flow conditions on membrane permeability, two complementary statistical approaches were applied. Welch's t-test allowed for a direct comparison of pooled group means across all experiments, revealing a large and statistically significant difference in FITC concentration between static and dynamic flow conditions (p = 0.0027, $\eta^2 = 0.6907$). This large effect size confirms a substantial reduction in permeability under dynamic flow. A mixed-model using Restricted Maximum Likelihood (REML) was applied to the three trials with same conditions and data (8,9,10). REML estimation improves variance component estimates by accounting for fixed effects before estimating random variance components, making it particularly useful for biological data with limited replicates or missing values. Although the Condition term approached significance (p = 0.0903), it did not surpass the conventional threshold. Nonetheless, the observed F-value (F(1,2) = 9.603) reflects a considerable proportion of explained variance. In general, the F-statistic quantifies the ratio of systematic variance (explained by the model) to unsystematic variance (residual error). Higher F-values suggest stronger group effects relative to background variability. Here, the trend mirrors the outcome of the Welch's test, reinforcing the interpretation of a biologically relevant effect that is underpowered in this subset. The nonsignificance in the controlled subset may stem from the small number of experiments (n = 3), limiting statistical power despite consistent effect direction. The agreement across analytical approaches strengthens the conclusion that dynamic flow reduces membrane permeability, even when experiment-level variability is considered.

Box 3: Summary: Permeability

- Breathing to cells significantly reduces FITC permeability compared to static conditions (p = 0.0027, $\eta^2 = 0.69$).
- The effect persists under controlled conditions, although not statistically significant due to sample limitations (p = 0.0697).
- Mixed-effects modelling accounts for random variance across experiments and samples.
- Both analyses support the hypothesis that cells reinforce barrier function.



TU Sibliothek, WIEN Your knowledge hub

Viability

Confocal z-stack analysis confirmed that cells were alive across all conditions, with no evidence of cell death in any examined area. However, further insights were provided by the colour-coded z-projections, which indicated that epithelial cells, particularly in the co-cultured condition, exhibited vertical migration within the tissue. While *Only H441* shows a penetration into the tissue of up to 100 µm (ref. 3.12), *Only HUVECs* show almost only one colour, which indicates that they remain on the surface. This spatial shift suggests a potential reorganization of the cell layer over time. The migration of epithelial cells into the membrane might not only indicate active interaction with the matrix but also contribute to altered mechanical properties—potentially increasing tissue stiffness. These findings offer mechanistic insights into how flow and co-culture conditions influence both viability and functional positioning of the cells.

Box 4: Summary: Viability

- Viability was confirmed across all experimental conditions using orthogonal z-projections.
- Colour-coded z-projections revealed vertical migration of epithelial cells within the tissue.

TU Sibliothek,

4.1 Limitations

Several methodological limitations should be acknowledged to provide a transparent context for the interpretation of the results: The biological membrane used in this study exhibited a thickness of approximately 100 µm, considerably exceeding the native alveolar barrier of about 2 µm. This discrepancy may influence both diffusion dynamics and local strain distribution. While the mechanical characterisation applied models derived from bulge tests, the specific geometric and viscoelastic properties of the collagen-elastin membranes deviate from the assumptions of these classical approaches. Consequently, derived mechanical parameters, such as the Young's modulus, should be considered approximate and primarily indicative of trends. The filter component used during cyclic breathing experiments showed minor effects on pressure transmission under normal conditions, based on preliminary tests. Nevertheless, in specific cases, such as severe filter blockage or use of a 0.2 µm pore size filter, notable pressure attenuation was observed. To mitigate this potential confounder, the filter was omitted during Trial 11 OCT measurements. The OCT system, while offering high-resolution imaging, allowed only the basal surface of the membranes to be reliably captured during dynamic deformation. Therefore, conclusions regarding strain distribution across the full membrane thickness must be drawn with caution. The statistical analysis, particularly of permeability assays, was limited by the small number of biological replicates. While strong trends were observed, broader sampling would be necessary to conclusively confirm these findings. Differences in vertical cell migration between epithelial and endothelial populations, observed qualitatively in viability assays, may influence local mechanical properties and diffusion barriers but were not quantified within this study. Environmental factors such as minor temperature or humidity variations during OCT measurements may have influenced membrane mechanical properties, although efforts were made to minimise these effects.

Summary

Box 5: Theses review

- × Realistic breathing mechanics: The collagen-elastin composition enables the recreation of alveolar breathing cycles (10% strain). For the corresponding pressure, the elastic modulus is in the range of kilo-pascals.
- ✓ Physiological strain distribution: The system distributes mechanical stress in a physiological gradient, ensuring that cells experience region-specific deformations, as seen in vivo.
- ✓ Influence of cells on mechanics: Lower strain levels are reached after epithelial and endothelial cells are added to the biological membrane. This highlights the interplay between tissues and cells.
- × Cellular strain: Beyond evaluating the biological membrane, the Optical Coherence Tomography technique allows to study cellular strain. This serves as a proof to validate.
- ✓ Influence of cells on permeability: The biological membranes show lower permeability levels when carrying confluent cell layers.

The mechanical characterisation of the collagen-elastin membranes in the acellular state revealed stiffness values within the kilopascal range, consistent with reported values for soft biological tissues. This finding supports the physiological relevance of the membrane architecture prior to



TU Sibliothek, WLEN Your knowledge hub

cellular interaction. However, after seeding with epithelial and endothelial cells, no elasticity was detectable within the sensitivity limits of the method, indicating substantial alteration of the membrane's mechanical properties due to cellular remodelling processes.

The study aimed to reconstruct physiologically realistic alveolar mechanics using a biologically functional membrane combined with a dynamic, pressure-driven actuation system. Special focus was placed on evaluating the influence of cells on both mechanical behaviour and barrier function. The integration of complementary methods—optical coherence tomography (OCT) for quantifying membrane strain, permeability assays for assessing barrier tightness, and viability measurements—served to establish a multidimensionally validated lung-on-chip environment responsive to tissue-level interactions. This methodological combination enabled the characterisation of both physical deformation and biological functionality under conditions resembling respiratory dynamics.

Whilst the system successfully achieved localised strains of approximately 10% in accordance with alveolar physiology, it should be noted that the membrane thickness of approximately 100 µm exceeds that of the native alveolar barrier (about 2 µm) by roughly a factor of 50. This discrepancy in structural scaling must be considered when interpreting both mechanical stress distribution and molecular transport phenomena. Nevertheless, the model's performance remains consistent with key physiological principles, as outlined in the summary of thesis objectives (see Box 5 as Fig.5.2).

In summary, the combination of imaging-based mechanical analysis, functional barrier assessment, and biological characterisation provides a holistic framework for evaluating dynamic *in vitro* lung models. The findings underline the importance of cross-methodological validation and highlight the physiologically significant role of cell–matrix interaction in shaping tissue-level function. Further investigations, particularly involving high-resolution structural collagen imaging, may elucidate the origins of regional heterogeneity and better explain the loss of measurable elasticity following cell integration. Due to methodological compromises in speed and precision, strain could not be resolved at the cellular level; however, a fluorescent *x*–*y* projection approach during breathing cycles might offer further insights.

e gedruckte Originalversion dieser Diplomarbeit	original version of this thesis is available in print
3ibliothek. Die approbiert	our knowledge hub The approved

Method	Acellular Membranes	Cell-Seeded Membranes		
OCT	Detectable elasticity, stiff-	No measurable elasticity;		
(Mechanical)	ness in the kilo-pascal	strain shielding by cellular		
	range.	layer.		
Permeability	High permeability to	Significant reduction in per-		
(Functional)	FITC-sodium.	meability due to tight cell		
		layer formation.		
Viability	-	Viability confirmed via dual		
(Functional)		staining (live/dead assay);		
		functional integrity main-		
		tained under dynamic strain.		

Recap of Methods The integration of strain measurement via OCT with functional assays such as FITC permeability provides a holistic picture of barrier function. The reduced strain observed in cell-seeded membranes aligns with increased barrier integrity, as confirmed by reduced FITC diffusion, thereby reinforcing the biological relevance of the combined model approach.



Appendix

Protocol of Membrane Production A.1

Mixing of the Components

As the main components of the CE membrane, rat-tail collagen type I (high concentration, Corning) and bovine neck elastin powder (lyophilised, salt-free, Sigma-Aldrich) are used in a 1:1 ratio.

Prior to starting, the desired total volume must be defined according to material availability. The coating volume per net is approximately 230 µL, rounded to 250 µL to ensure a working buffer.

Day 1: Preparation of Outer Coating

- Pre-cool the centrifuge to 4 °C.
- Prepare an ice container and place it inside the laminar flow hood along with sterile water, a closable box containing nets, and all solutions: PBS (pH 7.4), NaOH, MilliQ water, dissolved elastin (3.5 mg mL^{-1}), and collagen I.
- Mark two sterile 5 mL tubes for elastin and collagen preparation, and place them in the ice container.
- Transfer half of the total required volume of elastin into the elastin tube and return it to the

T Sibliothek, Vour knowledge hub

- Into the collagen tube:
 - Add PBS.
 - Neutralise with NaOH (1.5× the calculated amount for collagen neutralisation) and mix gently by pipetting up and down until the solution appears pink.
 - Add the collagen I stock solution and mix gently (avoiding bubble formation).
 - Verify pH using pH strips.
 - Add the calculated volume of sterile water and mix carefully.
- Centrifuge both tubes at 4 °C for 1 minute to remove residual bubbles.
- Combine the collagen and elastin solutions by gentle mixing.
- Apply the mixture dropwise onto the backside of the nets:
 - Droplet size must be carefully controlled to avoid coating failure (too small: time-consuming; too large: droplet weight may cause membrane perforation).
- Proceed net by net, mixing the solution gently between applications.
- Place the coated nets in a closable box and incubate for 90 minutes at 37 °C and 5% CO₂.
- After incubation, allow the box to cool inside the laminar flow hood before carefully opening it.

Day 2: Hydration Step

- Transfer wells into well plates.
- Hydrate the membranes by covering with sterile water for 4 hours (500 μL above and below the membrane).
- Carefully remove the water and allow membranes to dry under the laminar flow hood.

Day 3: Preparation of Inner Coating

• Repeat the coating procedure from Day 1, applying the solution to the inner side of the net.

Day 4: Hydration of Inner Coating

• Repeat the hydration procedure from Day 2.

Collagen Solution Preparation

The volume calculations for preparing the collagen solution are as follows:

$$V_{Col.Stock} = \frac{Desired\ concentration}{Stock\ concentration} \times Desired\ volume \tag{A.1}$$

$$V_{PBS} = \frac{Desired\ volume}{10} \tag{A.2}$$

$$V_{NaOH} = 0.023 \times V_{Col.Stock} \tag{A.3}$$

$$V_{H_2O} = Desired \ volume - V_{Col.Stock} - V_{PBS} - V_{NaOH}$$
(A.4)

Challenge: Avoid too many coatings at once. Collagen is hardening quickly. A long procedure might risk redundancy of the membranes. Also, the pH value should be tracked consistently. As known, the properties of collagen-based hydrogels depend on it [31, 32].

A.2 Cells

Cell Culture

Cells are cultured with the listed medium, which is changed every two days and 1:100 Penicillin-Streptomycin is added to all media to suppress undesired infection. Confluency 1 is daily checked by light microscopy. H441 (Epithelial cells) take by experience one week to get confluent, HUVECs (Endothelial cells) around five days. Maintaining the proliferation phenotype, cells were passaged (harvested and seeded in a new culture dish), when about 80 - 90% of the dish was filled. For HUVECs, passages 1 - 3 are used. For H441, passages up to 45 are used (This experiment: 38 - 45).

¹The portion of space of the culture dish covered by adherent cells

Harvesting H441 Cells from a confluent T75 Flask

Medium preparation: RPMI-1640 Medium + 5% fetal bovine serum (FBS) + 1:100 Penicillin-Streptomycin (10,000 U/ml)

- Wash the cells with 10 mL of PBS (-/-) once.
- Add 2 mL of 0.25% Trypsin and 1 mM EDTA in PBS (-/-).
- Incubate the cells for 3 minutes at 37°C. The incubation time varies depending on the confluency of the layer. Within 5-7 minutes, cells should detach completely.
- Stop the trypsin activity with 10 mL of PBS (+/+) + 5% FBS, collect the cells, and centrifuge at 200 x g for 5 min.
- After centrifugation, discard the supernatant, resuspend the pellet in 1 mL of RPMI medium, and count.
- For counting, use a 1:10 dilution (90 μL medium + 10 μL resuspended cell) and count the cells 1:1 with the cell counter (10 μL of Trypan Blue and 10 μL of the 1:10 diluted cells).
- Medium exchange: 15 mL of prepared medium.

Harvesting HUVECs from a confluent T25 Flask

Medium preparation: Endothelial Cell Growth Medium MV (EC-Medium) + supplements inside + 1:100 Penicillin-Streptomycin (10,000 U/ml)

- Wash with 5 mL of Dulbecco's phosphate-buffered saline without magnesium and calcium PBS (-/-).
- Add 1 mL of 0.25% trypsin and 1 mM EDTA in PBS (-/-) and incubate for 3 min at 37°C.
- Stop trypsin activity by adding 5 mL of PBS (+/+) and 5% FCS.
- Centrifuge at 300 x g for 5 minutes at room temperature (RT) in a 50-mL conical tube. Remove the supernatant and resuspend the cell pellet in 1 mL of EC medium.
- For counting, use a 1:10 dilution (90 μL medium + 10 μL resuspended cell) and count the cells 1:1 with the cell counter (10 μL of Trypan Blue and 10 μL of the 1:10 diluted cells).
- Medium exchange: 5 mL of prepared medium.

Cell Seeding and Cyclic Breathing

Day 0: Preparing for the Breathing Experiment To ensure proper hydration and mechanical flexibility, the chip is placed in culture medium overnight. This step is crucial to soften the biological membrane, allowing cells to attach more effectively in the following steps.

Day 1: Initial Epithelial Cell Seeding 500,000 epithelial cells (NCI-H441), outcome of a harvesting process (ref. A.2) are carefully pipetted onto the membrane at the inner side of the well. The cells are in 200 μL RPMI and 10% FBS. The cells are evenly distributed to promote uniform attachment and growth. The well is then placed in the incubator to allow the cells to settle and adhere. 500 μL of medium is added on the endothelial side, 300 μL on the epithelial side (500 μL in total.

Day 2: Medium Exchange and NourishmentFresh culture medium (RPMI and 10% FBS) is gently exchanged to remove unattached cells and provide essential nutrients for cell proliferation and viability.

Day 3: Additional Epithelial Cell Seeding on the Outer Membrane 500,000 endothelial cells are seeded on the outer side of the membrane. The cells are in 200 μL EC and 10% FBS. The cells are evenly distributed to promote uniform attachment and growth. To ensure successful adhesion, the well is left inverted inside the incubator for 1.5 hours.

Day 4: Establishing the Air-Liquid Interface (ALI)The medium level is adjusted so that only the basal side of the endothelial layer remains submerged, exposing the apical side to air. The portion of FBS within the EC medium is increased to 20% to promote proliferation.

Day 5: Dynamic and Static Conditions

Dynamic group (ref.1.2.4): The net is embedded in the sterilized chip. Supported by medium from the endothelial side. The breathing system, simulating physiological breathing movements, is adapted and checked by light microscopy (is there any movement visible at the edge of the nets?).

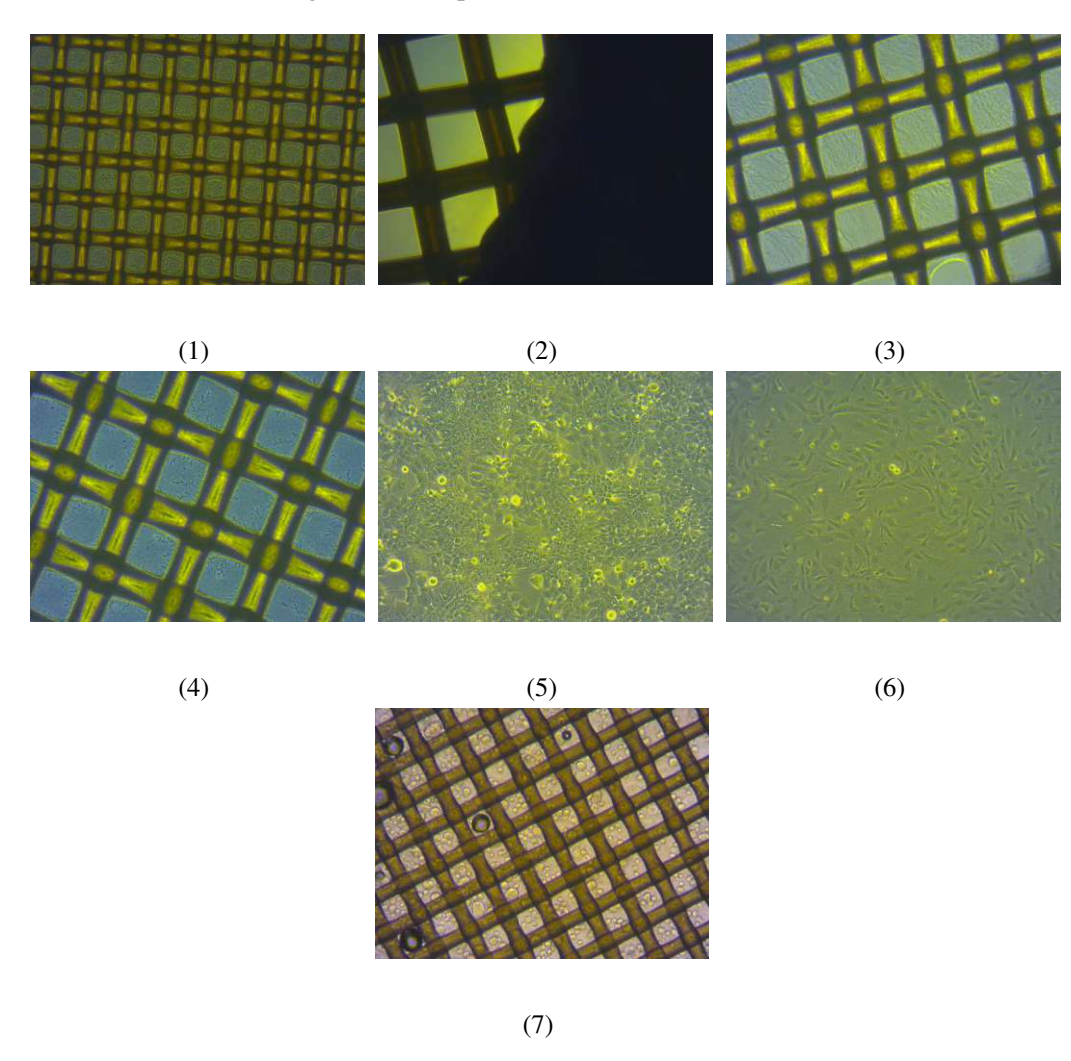
Static and Control group: The well remains in an incubator environment without mechanical stimulation. Medium is exchanged daily by the same quantity as for the Dynamic group.

Day 6 and Day 7: Sustaining the CultureFresh medium is exchanged to maintain cell health and promote further differentiation.

Day 8: Experiment Termination and Sample CollectionThe experiment part of cyclic breathing concludes, further analysis, including imaging and functional assays, begins.

A.3 Supportive Microscopy

Images were taken regularly to verify the steps of the coating and the cell phase. Irregularities, especially during the coating (bubbles, uneven coverage, thin coating, rough edges), led to the discard of the sample. If one layer was coated, additional information about the coating quality of the second layer is reduced as they lay on the same plane. Same holds for the endothelial cells, which were hidden in the light microscope.



A1: Microscopy images of coatings and cells: 1) Coating 2) Coating with hole 3) Salt structure within tissue 4) Rough edge of multi-used well 5) Endothelial cells after 7 days of culturing in the flask 6) Epithelial cells after 7 days of culturing in the flask 7) Freshly seeded epithelial cells

A.4 OCT System Description

The Optical Coherence Tomography (OCT) system used in this study is the *Thorlabs Ganymede OCT-UHR601-SP1*, a high-resolution spectral domain OCT device with the following specifications:

- Center wavelength: 750 nm
- A-Scan / Line Rate: max. 248 kHz
- Adjustable A-Scan Rate with seven different speeds
- Integrated reference arm for common-path configurations
- Axial resolution: <1.2 µm in air
- Lateral resolution: 2 μm (Mitutoyo NIR 20x lens) or 4 μm (Mitutoyo NIR 10x lens)
- Field of view: 2.5 mm x 2.5 mm (20x) or 4 mm x 4 mm (10x)
- Measurement depth: >700 μm in air
- Light source: Supercontinuum light source
- Motion detection via Doppler and Speckle Variance Mode

A.5 Code for TIFF File Processing

```
3ibliothek, ween your knowledge hub
```

```
for i, page in enumerate(stack.pages):
                            img = page.asarray()
                            png_path = os.path.join(output_folder, \
                            f"{os.path.splitext(file)[0]}_frame_{i_+_1}.png")
                            Image.fromarray(img).save(png_path)
                    os.remove(tiff_path)
                    print(f"Converted_'{file}'_to_PNG_and_saved_in_'{output_folder}'.")
                except Exception as e:
                    print(f"Error_processing_'{file}':_{e}")
def calculate_center_of_mass(image):
    #Calculates the vertical center of mass (y_center) of an image based on pixel intensities
    if image.ndim > 2:
        image = np.mean(image, axis=-1)
    height, width = image.shape
    y_indices = np.arange(height)
    intensity_sum = np.sum(image)
    if intensity_sum == 0:
        return height // 2
    y_center = np.sum(y_indices[:, None] * image) / intensity_sum
def find_extreme_frames(images):
   \#Finds the frames in the image series where a structure moves to its highest \setminus
   and lowest vertical positions based on the center of mass
    center_of_mass_positions = [calculate_center_of_mass(image) for image in images]
    return np.argmin(center_of_mass_positions), np.argmax(center_of_mass_positions)
def add_scale_bar(image, pixel_size_x, pixel_size_z, scale_bar_length_um=100):
    #Adds a scale bar to the bottom-right corner of the image
    draw = ImageDraw.Draw(image)
    scale_bar_length_px_x = int((scale_bar_length_um / 1000) / pixel_size_x)
    scale_bar_length_px_z = int((scale_bar_length_um / 1000) / pixel_size_z)
    bar_thickness = 5
    image_width, image_height = image.size
    x_start = image_width - scale_bar_length_px_x - 20
    x_{end} = image_width - 20
    y_start = image_height - 20 - bar_thickness
    y_end = image_height - 20
    draw.rectangle([x_start, y_start, x_end, y_end], fill="white")
    z_x_{start} = image_width - 20 - bar_thickness
    z_x_{end} = image_width - 20
    z_y_start = image_height - scale_bar_length_px_z - 20
    z_y_end = image_height - 20
    draw.rectangle([z_x_start, z_y_start, z_x_end, z_y_end], fill="white")
    text = f"{scale_bar_length_um}"
    font = ImageFont.truetype("arial.ttf", size=20)
    text_bbox = draw.textbbox((0, 0), text, font=font)
    text_x = x_start - (text_bbox[2] - text_bbox[0]) - 10
```

```
TU Sibliothek,
WEN Your knowledge hub
```

```
text_y = y_start + (bar_thickness // 2) - ((text_bbox[3] - text_bbox[1]) // 2)
    draw.text((text_x, text_y), text, fill="white", font=font)
    return image
def process_tiff_with_scale_bar(reduced_data, input_main_folder, output_main_folder):
    #Adds a scale bar to the reduced TIFF images and saves them in their original subfolder structure
    os.makedirs(output_main_folder, exist_ok=True)
    ri = 1.4
    pixel_size_x = 0.000490
    pixel_size_z = 0.000686 / ri
    for tiff_path, images in reduced_data.items():
        root = os.path.dirname(tiff path)
        file = os.path.basename(tiff_path)
        metadata = read_metadata(os.path.join(root, "extracted_Metadata.txt"))
        folder_name = metadata.get("Comment", "default")
        study_name = metadata.get("Study", "default")
        a_scans = metadata.get("AScans", "Unknown")
        output_folder = os.path.join(output_main_folder, f"{study_name}_{folder_name}", \
        os.path.relpath(root, input_main_folder))
        os.makedirs(output_folder, exist_ok=True)
        update_metadata(metadata, pixel_size_x, pixel_size_z)
        output metadata path = os.path.join(output folder, "extracted Metadata.txt")
        with {\bf open}\,({\tt output\_metadata\_path},\ '\,{\tt w'}\,) as meta:
            meta.writelines(metadata.values())
        base_name, ext = os.path.splitext(file)
        new_filename = f"{base_name}_AScans_{a_scans}{ext}"
        output_tiff_path = os.path.join(output_folder, new_filename)
        with tiff.TiffWriter(output_tiff_path, bigtiff=True) as writer:
            for img in (Image.fromarray(img).rotate(-90, expand=True) for img in images):
                writer.write(np.array(add_scale_bar(img, pixel_size_x, pixel_size_z)))
        def get_next_sample_count(output_folder, base_filename):
    \# Determines the next available sample count (n1, n2, ...) for the given base filename
    existing_files = os.listdir(output_folder) if os.path.exists(output_folder) else []
    count_pattern = re.compile(rf"{re.escape(base_filename)}_n(\d+)_")
    existing_counts = [int(match.group(1)) for file in existing_files if (match := count_pattern.search(file))]
    return f"n{max(existing_counts,_default=0)_+_1}"
def process_tiff_with_extremes(input_main_folder, output_main_folder):
    os.makedirs(output_main_folder, exist_ok=True)
    unique_number = input("Enter_a_unique_number_to_include_in_the_file_names:_").strip()
    ri = 1.4
    pixel_size_x = 0.000490
    pixel\_size\_z = 0.000686 / ri
    for root, dirs, files in os.walk(input_main_folder):
        for file in files:
            if file.lower().endswith(('.tiff', '.tif')):
```

```
3ibliothek, Wur knowledge hub
```

```
tiff_path = os.path.join(root, file)
                with tiff.TiffFile(tiff_path) as stack:
                    images = stack.asarray()
                min_index, max_index = find_extreme_frames(images)
                min_frame = Image.fromarray(images[min_index]).rotate(-90, expand=True)
                max_frame = Image.fromarray(images[max_index]).rotate(-90, expand=True)
                metadata = read_metadata(os.path.join(root, "extracted_Metadata.txt"))
                folder_name = metadata.get("Comment", "default")
                study_name = metadata.get("Study", "default")
                output_folder = output_main_folder
                os.makedirs(output_folder, exist_ok=True)
                base_filename = f"{unique_number}_{study_name}_{folder_name}"
                sample_count = get_next_sample_count(output_folder, base_filename)
                min_filename = f"{base_filename}_{sample_count}_down_{min_index}.png"
                max_filename = f"{base_filename}_{sample_count}_up_{max_index}.png"
                min_frame.save(os.path.join(output_folder, min_filename))
                max_frame.save(os.path.join(output_folder, max_filename))
                print(f"Saved_extreme_frames_with_unique_numbering:_{min_filename},_{max_filename}")
def reduce_timeseries_images(input_main_folder):
    #Reduce the image to save memory
    Returns:
        reduced_data (dict): {tiff_path: [reduced images as NumPy arrays]}
    reduced data = {}
    for root, dirs, files in os.walk(input_main_folder):
        for file in files:
            if (file.lower().endswith(('.tiff', '.tif')) and ("OCT-Stack" in file or "OCT-Tiff-Camera" in file)):
                tiff_path = os.path.join(root, file)
                with tiff.TiffFile(tiff_path) as stack:
                    images = [page.asarray() for page in stack.pages]
                    if "OCT-Tiff-Camera" in file or len(images) <= 150:</pre>
                        reduced_data[tiff_path] = images
                    else:
                        reduced_data[tiff_path] = images[:150]
    return reduced_data
def read_metadata(metadata_file):
    \# Reads the metadata from the specified file and returns a dictionary
    metadata = defaultdict(str)
    if os.path.exists(metadata_file):
        with open(metadata_file, 'r') as meta:
            for line in meta:
                for key in ("Comment:", "Study:", "AScans:"):
                    if line.startswith(key):
                       metadata[key[:-1]] = line.split(key)[1].strip()
    return metadata
def update_metadata(metadata, pixel_size_x, pixel_size_z):
```

```
Sibliothek, Diviewed Your knowledge hub
```

```
#Updates the metadata dictionary with the new pixel sizes

metadata["SizeX"] = f"{pixel_size_z}"

metadata["SizeZ"] = f"{pixel_size_x}"

if __name__ == "__main__":
    input_main_folder = input("Enter_path_to_input_main_folder:_").strip()
    output_main_folder = input("Enter_path_to_output_main_folder_for_processed_TIFFs:_").strip()
    output_extreme_folder = input("Enter_path_to_output_folder_for_extreme_frames:_").strip()

print("Converting_'OCT-Tiff-Camera'_files_to_PNG...")
    convert_tiff_camera_to_png(input_main_folder, output_main_folder)

print("Reducing_time-series_and_processing_TIFF_files_with_scale_bar...")
    reduced_data = reduce_timeseries_images(input_main_folder)
    process_tiff_with_scale_bar(reduced_data, input_main_folder, output_main_folder)

print("Processing_extreme_frames...")
    process_tiff_with_extremes(input_main_folder, output_extreme_folder)

print("Processing_complete.")
```

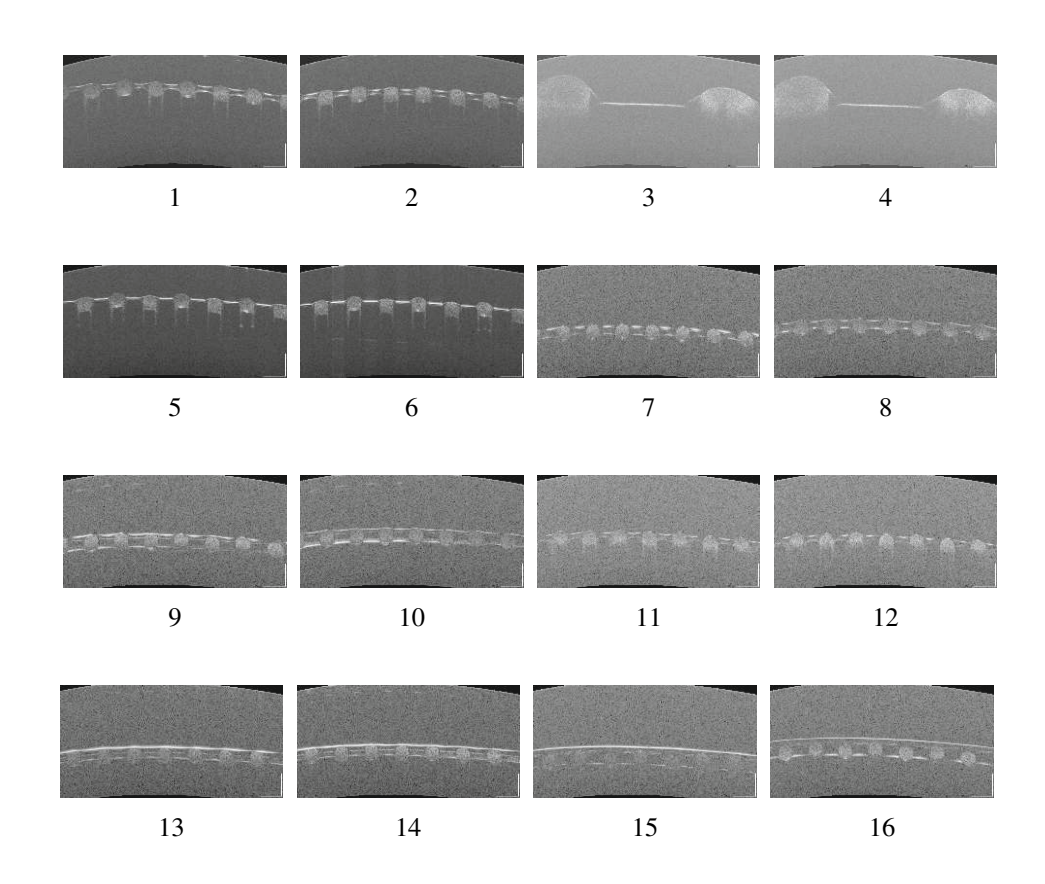
OCT Images **A.6**

A.6.1**Pre-tests**

Due to the variability of the test conditions, a legend for these pre-tests would not provide additional clarity.

New Filename	Original Filename
1	5_lab_on_a_chip_nass_klein_doppelt_None_n1_down_79.png
2	5_lab_on_a_chip_nass_klein_doppelt_None_n1_up_59.png
3	5_lab_on_a_chip_trocken_gross_einfach_None_n1_down_48.png
4	5_lab_on_a_chip_trocken_gross_einfach_None_n1_up_66.png
5	5_lab_on_a_chip_trocken_klein_doppelt_None_n1_down_73.png
6	5_lab_on_a_chip_trocken_klein_doppelt_None_n1_up_17.png
7	6_lab_on_a_chip_nass_15_Tage_nr1_filter_10mbar_none_n1_down_419.png
8	6_lab_on_a_chip_nass_15_Tage_nr1_filter_10mbar_none_n1_up_312.png
9	6_lab_on_a_chip_nass_15_Tage_nr1_none_n1_down_120.png
10	6_lab_on_a_chip_nass_15_Tage_nr1_none_n1_up_95.png
11	6_lab_on_a_chip_nass_15_Tage_nr1_super_filter_10mbar_none_n1_down_52.png
12	6_lab_on_a_chip_nass_15_Tage_nr1_super_filter_10mbar_none_n1_up_161.png
13	6_lab_on_a_chip_nass_15_Tage_nr2_none_n1_down_281.png
14	6_lab_on_a_chip_nass_15_Tage_nr2_none_n1_up_133.png
15	6_lab_on_a_chip_nass_3_Tage_nr3_none_n1_down_22.png
16	6_lab_on_a_chip_nass_3_Tage_nr3_none_n1_up_127.png

Table A.1: OCT pre-tests: Filename conversion



A2: OCT images: pre-tests

A.6.2**Main Tests**

Note:

11	Dyn yes_1	10bpm	n2	down	73.png
Trial	Sample condition* _ no.	Parameter**	Mode***	Position****	Original <i>TIFF</i> -file****

Table A.2: Overview of trial conditions and corresponding file references.

Table A.3: OCT main tests: Filename conversion

New Filename	Original Filename
1	11_Dyn_yes1_10bpm_n2_down_73.png
2	11_Dyn_yes1_10bpm_n2_up_9.png
3	11_Dyn_yes1_10mbar_n2_down_7.png
4	11_Dyn_yes1_10mbar_n2_up_27.png
5	11_Dyn_yes1_15bpm_n2_down_9.png
6	11_Dyn_yes1_15bpm_n2_up_52.png
7	11_Dyn_yes1_15mbar_n2_down_34.png
8	11_Dyn_yes1_15mbar_n2_up_9.png
9	11_Dyn_yes1_1_3_n2_down_1.png
10	11_Dyn_yes1_1_3_n2_up_18.png
11	11_Dyn_yes1_20bpm_n2_down_28.png
12	11_Dyn_yes1_20bpm_n2_up_57.png
13	11_Dyn_yes1_30bpm_n2_down_37.png
14	11_Dyn_yes1_30bpm_n2_up_43.png
15	11_Dyn_yes1_5mbar_n2_down_45.png
16	11_Dyn_yes1_5mbar_n2_up_39.png
17	11_Dyn_yes1_7.5bpm_n2_down_398.png
18	11_Dyn_yes1_7.5bpm_n2_up_308.png
19	11_Dyn_yes1_7.5mbar_n2_down_6.png
20	11_Dyn_yes1_7.5mbar_n2_up_5.png
21	11_Dyn_yes1_rand_n2_down_0.png

^{*} Dynamic, Static, Control (A.2)

^{**} Change of Parameter (3.2), rand = edge

^{***} Example: One acquisition without averaging, another one with averaging (but no averaging images listed)

^{****} Mid, 1/3, Edge (fig. 2.6)

^{*****} Position within TIFF file sequence before conversion (2.4.2)

22	11_Dyn_yes1_rand_n2_up_54.png
23	11_Dyn_yes2_10bpm_n2_down_40.png
24	11_Dyn_yes2_10bpm_n2_up_51.png
25	11_Dyn_yes2_10mbar_n2_down_9.png
26	11_Dyn_yes2_10mbar_n2_up_57.png
27	11_Dyn_yes2_15bpm_n2_down_42.png
28	11_Dyn_yes2_15bpm_n2_up_51.png
29	11_Dyn_yes2_15mbar_n2_down_42.png
30	11_Dyn_yes2_15mbar_n2_up_7.png
31	11_Dyn_yes2_1_3_n2_down_41.png
32	11_Dyn_yes2_1_3_n2_up_65.png
33	11_Dyn_yes2_2.5mbar_n2_down_35.png
34	11_Dyn_yes2_2.5mbar_n2_up_75.png
35	11_Dyn_yes2_20bpm_n2_down_45.png
36	11_Dyn_yes2_20bpm_n2_up_32.png
37	11_Dyn_yes2_30bpm_n2_down_40.png
38	11_Dyn_yes2_30bpm_n2_up_17.png
39	11_Dyn_yes2_5mbar_n2_down_19.png
40	11_Dyn_yes2_5mbar_n2_up_39.png
41	11_Dyn_yes2_7.5bpm_n2_down_32.png
42	11_Dyn_yes2_7.5bpm_n2_up_101.png
43	11_Dyn_yes2_7.5mbar_n2_down_35.png
44	11_Dyn_yes2_7.5mbar_n2_up_63.png
45	11_Dyn_yes2_rand_n2_down_59.png
46	11_Dyn_yes2_rand_n2_up_51.png
47	11_Stat_no1_10mbar, 10bpm_n2_down_86.png
48	11_Stat_no1_10mbar, 10bpm_n2_up_11.png
49	11_Stat_no1_10mbar, 15bpm_n2_down_58.png
50	11_Stat_no1_10mbar, 15bpm_n2_up_80.png
51	11_Stat_no1_10mbar, 20bpm_n2_down_47.png
52	11_Stat_no1_10mbar, 20bpm_n2_up_17.png
53	11_Stat_no1_10mbar, 30bpm_n2_down_58.png
54	11_Stat_no1_10mbar, 30bpm_n2_up_12.png
55	11_Stat_no1_10mbar, 7.5bpm_n2_down_24.png
56	11_Stat_no1_10mbar, 7.5bpm_n2_up_8.png
57	11_Stat_no1_10mbar_n2_down_13.png

58	11_Stat_no1_10mbar_n2_up_56.png
59	11_Stat_no1_15mbar_n2_down_7.png
60	11_Stat_no1_15mbar_n2_up_59.png
61	11_Stat_no1_1_3_n2_down_40.png
62	11_Stat_no1_1_3_n2_up_17.png
63	11_Stat_no1_2mbar_n2_down_63.png
64	11_Stat_no1_2mbar_n2_up_15.png
65	11_Stat_no1_5mbar_n2_down_46.png
66	11_Stat_no1_5mbar_n2_up_17.png
67	11_Stat_no1_7.5mbar_n2_down_89.png
68	11_Stat_no1_7.5mbar_n2_up_19.png
69	11_Stat_no1_rand_n2_down_14.png
70	11_Stat_no1_rand_n2_up_10.png
71	11_Stat_no2_10 bpm_n2_down_14.png
72	11_Stat_no2_10 bpm_n2_up_46.png
73	11_Stat_no2_10 mbar_n2_down_9.png
74	11_Stat_no2_10 mbar_n2_up_25.png
75	11_Stat_no2_15 bpm_n2_down_34.png
76	11_Stat_no2_15 bpm_n2_up_88.png
77	11_Stat_no2_15 mbar_n2_down_13.png
78	11_Stat_no2_15 mbar_n2_up_10.png
79	11_Stat_no2_1_3_n2_down_48.png
80	11_Stat_no2_1_3_n2_up_31.png
81	11_Stat_no2_2.5 mbar_n2_down_10.png
82	11_Stat_no2_2.5 mbar_n2_up_7.png
83	11_Stat_no2_20 bpm_n2_down_31.png
84	11_Stat_no2_20 bpm_n2_up_2.png
85	11_Stat_no2_30 bpm_n2_down_29.png
86	11_Stat_no2_30 bpm_n2_up_40.png
87	11_Stat_no2_5 mbar_n2_down_38.png
88	11_Stat_no2_5 mbar_n2_up_53.png
89	11_Stat_no2_7.5 bpm_n2_down_10.png
90	11_Stat_no2_7.5 bpm_n2_up_53.png
91	11_Stat_no2_7.5 mbar_n2_down_1.png
92	11_Stat_no2_7.5 mbar_n2_up_131.png
93	11_Stat_no2_rand_n2_down_35.png

94	11_Stat_no2_rand_n2_up_55.png
95	11_Stat_yes1_10bpm_n2_down_64.png
96	11_Stat_yes1_10bpm_n2_up_46.png
97	11_Stat_yes1_10mbar_n2_down_16.png
98	11_Stat_yes1_10mbar_n2_up_51.png
99	11_Stat_yes1_15bpm_n2_down_4.png
100	11_Stat_yes1_15bpm_n2_up_144.png
101	11_Stat_yes1_15mbar_n2_down_83.png
102	11_Stat_yes1_15mbar_n2_up_73.png
103	11_Stat_yes1_1_3_n2_down_73.png
104	11_Stat_yes1_1_3_n2_up_15.png
105	11_Stat_yes1_2.5mbar_n2_down_43.png
106	11_Stat_yes1_2.5mbar_n2_up_79.png
107	11_Stat_yes1_20bpm_n2_down_13.png
108	11_Stat_yes1_20bpm_n2_up_50.png
109	11_Stat_yes1_30bpm_n2_down_62.png
110	11_Stat_yes1_30bpm_n2_up_55.png
111	11_Stat_yes1_5mbar_n2_down_52.png
112	11_Stat_yes1_5mbar_n2_up_1.png
113	11_Stat_yes1_7.5bpm_n2_down_64.png
114	11_Stat_yes1_7.5bpm_n2_up_101.png
115	11_Stat_yes1_7.5mbar_n2_down_51.png
116	11_Stat_yes1_7.5mbar_n2_up_20.png
117	11_Stat_yes1_rand_n2_down_34.png
118	11_Stat_yes1_rand_n2_up_7.png
119	11_Stat_yes2_10 bpm_n2_down_112.png
120	11_Stat_yes2_10 bpm_n2_up_79.png
121	11_Stat_yes2_10mbar_n2_down_15.png
122	11_Stat_yes2_10mbar_n2_up_46.png
123	11_Stat_yes2_15 bpm_n2_down_105.png
124	11_Stat_yes2_15 bpm_n2_up_2.png
125	11_Stat_yes2_15mbar_n2_down_48.png
126	11_Stat_yes2_15mbar_n2_up_58.png
127	11_Stat_yes2_1_3_n2_down_74.png
128	11_Stat_yes2_1_3_n2_up_44.png
129	11_Stat_yes2_2.5mbar_n2_down_57.png

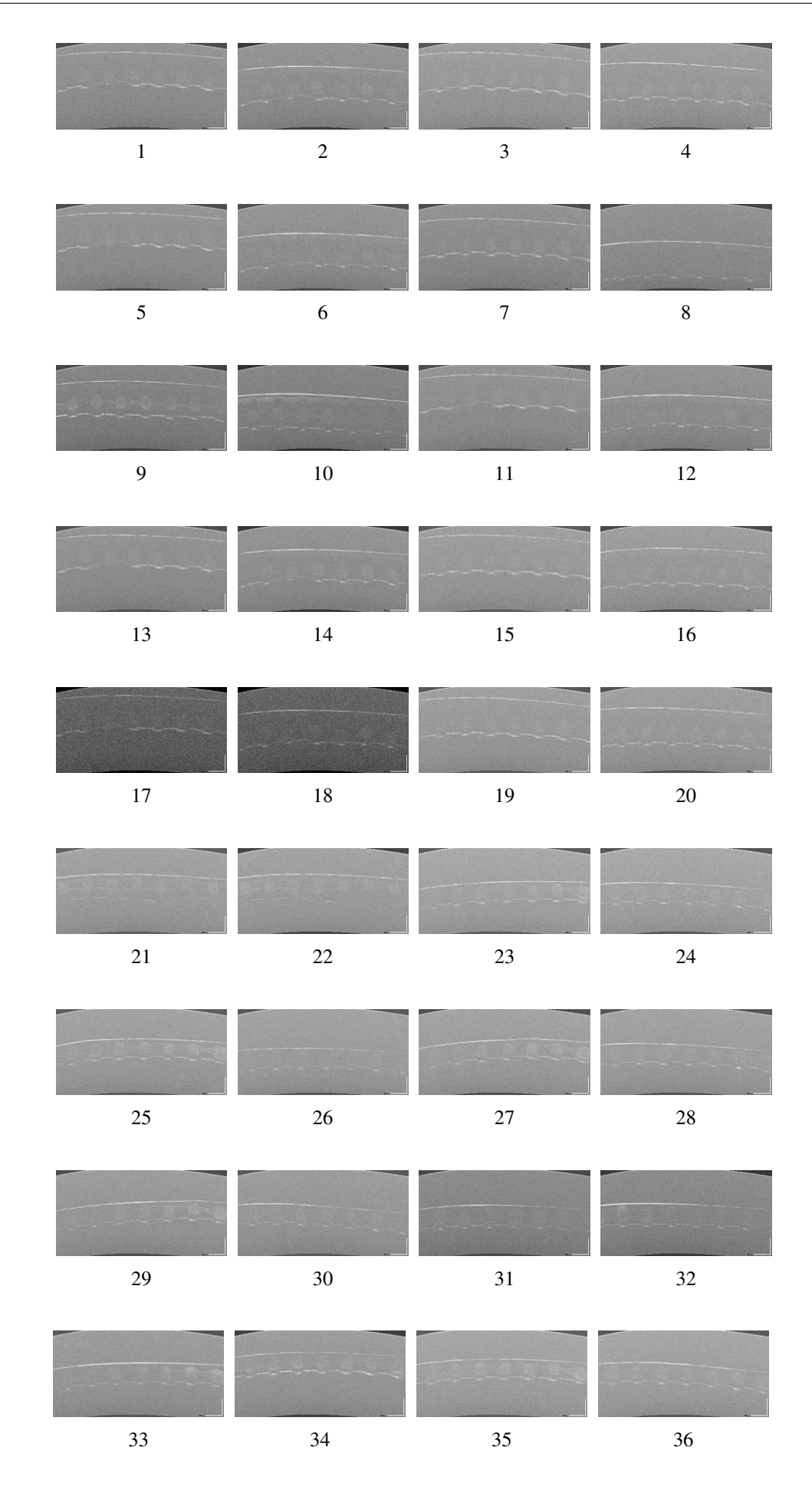
130	11_Stat_yes2_2.5mbar_n2_up_44.png
131	11_Stat_yes2_20 bpm_n2_down_87.png
132	11_Stat_yes2_20 bpm_n2_up_32.png
133	11_Stat_yes2_30 bpm_n2_down_49.png
134	11_Stat_yes2_30 bpm_n2_up_9.png
135	11_Stat_yes2_5mbar_n2_down_16.png
136	11_Stat_yes2_5mbar_n2_up_44.png
137	11_Stat_yes2_7.5 bpm_n2_down_52.png
138	11_Stat_yes2_7.5 bpm_n2_up_22.png
139	11_Stat_yes2_7.5mbar_n2_down_2.png
140	11_Stat_yes2_7.5mbar_n2_up_84.png
141	11_Stat_yes2_rand_n2_down_173.png
142	11_Stat_yes2_rand_n2_up_187.png
143	8_Dyn_1_10mbar_n2_down_165.png
144	8_Dyn_1_10mbar_n2_up_56.png
145	8_Dyn_1_6mbar_n1_down_10.png
146	8_Dyn_1_6mbar_n1_up_33.png
147	8_Dyn_2_10mbar, neuer Filter_n1_down_356.png
148	8_Dyn_2_10mbar, neuer Filter_n1_up_35.png
149	8_Dyn_2_10mbar, neuer Filter_n2_down_202.png
150	8_Dyn_2_10mbar, neuer Filter_n2_up_344.png
151	8_Dyn_2_20mbar_n2_down_123.png
152	8_Dyn_2_20mbar_n2_up_25.png
153	8_Dyn_2_6mbar, neuer Filter_n1_down_141.png
154	8_Dyn_2_6mbar, neuer Filter_n1_up_164.png
155	8_Dyn_2_None_n1_down_197.png
156	8_Dyn_2_None_n1_up_535.png
157	8_Stat_2_50mbar, neuer Filter_n1_down_196.png
158	8_Stat_2_50mbar, neuer Filter_n1_up_67.png
159	8_Stat_no1_10mbar_n1_down_89.png
160	8_Stat_no1_10mbar_n1_up_124.png
161	9_Dyn_1_10mbar_n1_down_212.png
162	9_Dyn_1_10mbar_n1_up_190.png
163	9_Dyn_1_15mbar_n1_down_127.png
164	9_Dyn_1_15mbar_n1_up_183.png
165	9_Dyn_1_15mbar_n2_down_177.png

xviii

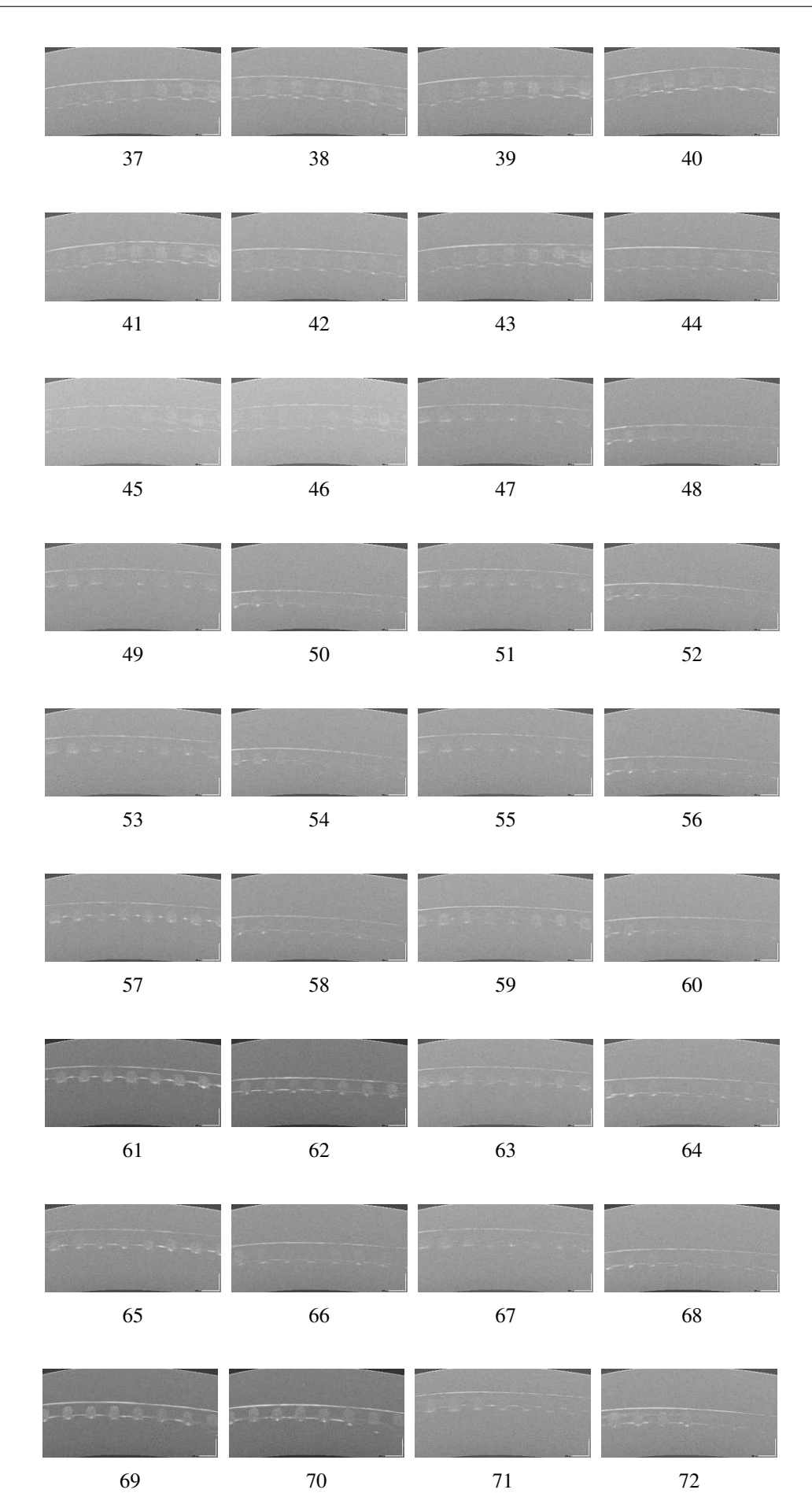
₹
<u>e</u>
£ §
dg ee
ow e
= {
M §
Z

166	9_Dyn_1_15mbar_n2_up_154.png
167	9_Dyn_2_H441_10mbar_n1_down_159.png
168	9_Dyn_2_H441_10mbar_n1_up_105.png
169	9_Dyn_2_H441_10mbar_n2_down_9.png
170	9_Dyn_2_H441_10mbar_n2_up_33.png
171	9_Dyn_2_H441_15mbar_n1_down_0.png
172	9_Dyn_2_H441_15mbar_n1_up_42.png
173	9_Dyn_2_H441_15mbar_n2_down_183.png
174	9_Dyn_2_H441_15mbar_n2_up_63.png
175	9_Dyn_3_HUV_10mbar_n1_down_160.png
176	9_Dyn_3_HUV_10mbar_n1_up_200.png
177	9_Dyn_3_HUV_15mbar_n1_down_32.png
178	9_Dyn_3_HUV_15mbar_n1_up_146.png
179	9_Stat_1_10mbar_n1_down_117.png
180	9_Stat_1_10mbar_n1_up_146.png
181	9_Stat_2_10mbar, 1_3_n1_down_560.png
182	9_Stat_2_10mbar, 1_3_n1_up_748.png
183	9_Stat_2_10mbar, Rand_n1_down_266.png
184	9_Stat_2_10mbar, Rand_n1_up_238.png
185	9_Stat_2_10mbar_n1_down_104.png
186	9_Stat_2_10mbar_n1_up_10.png
187	9_Stat_3_10mbar, ohne filter_n1_down_44.png
188	9_Stat_3_10mbar, ohne filter_n1_up_105.png
189	9_Stat_3_10mbar_n1_down_53.png
190	9_Stat_3_10mbar_n1_up_153.png
191	9_Stat_no1_10 mbar_n1_down_184.png
192	9_Stat_no1_10 mbar_n1_up_60.png
193	9_Stat_no1_15 bpm_n1_down_237.png
194	9_Stat_no1_15 bpm_n1_up_199.png
195	9_Stat_no1_15 mbar_n1_down_66.png
196	9_Stat_no1_15 mbar_n1_up_104.png

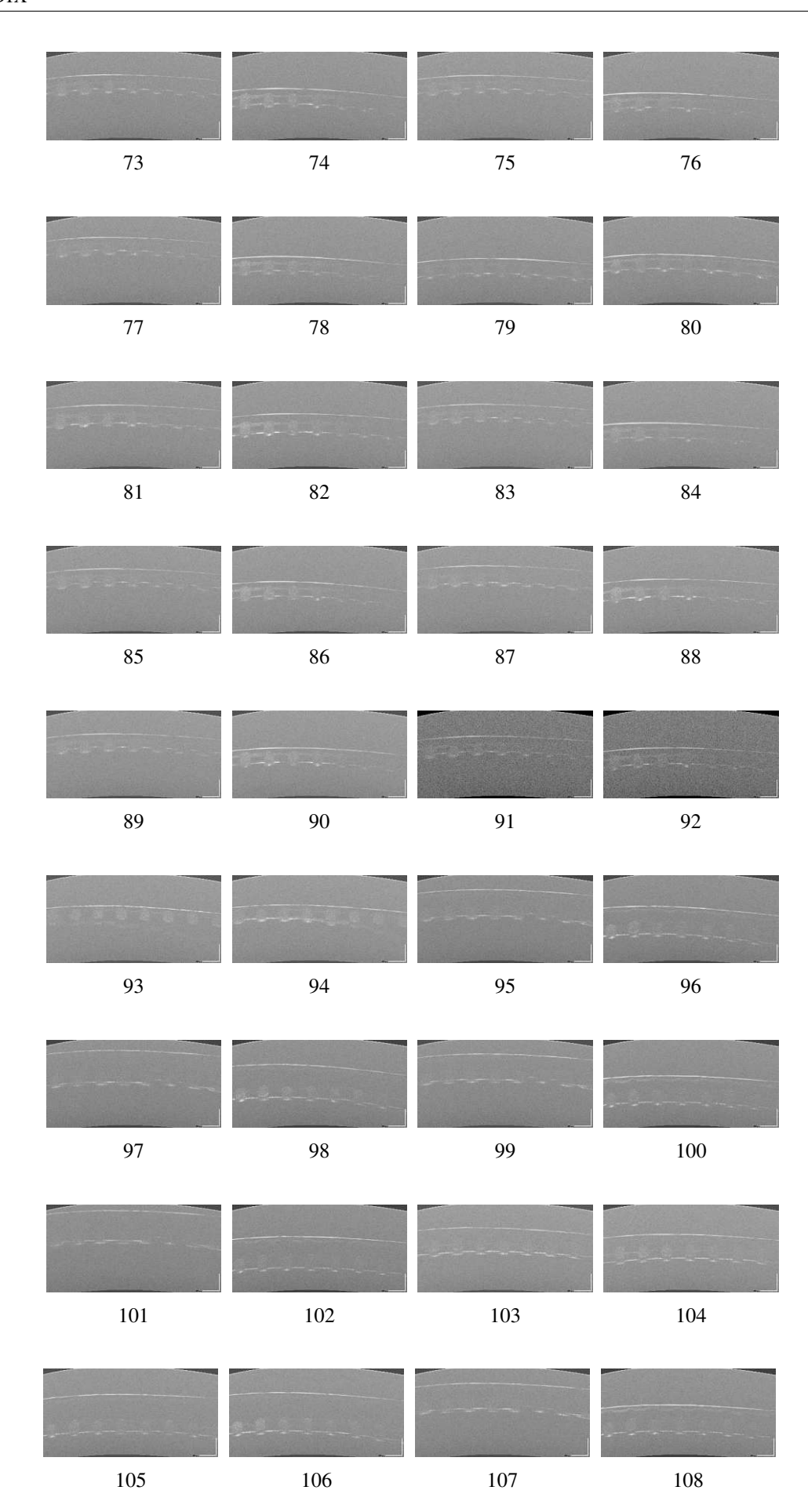
 $\mathbf{X}\mathbf{X}$



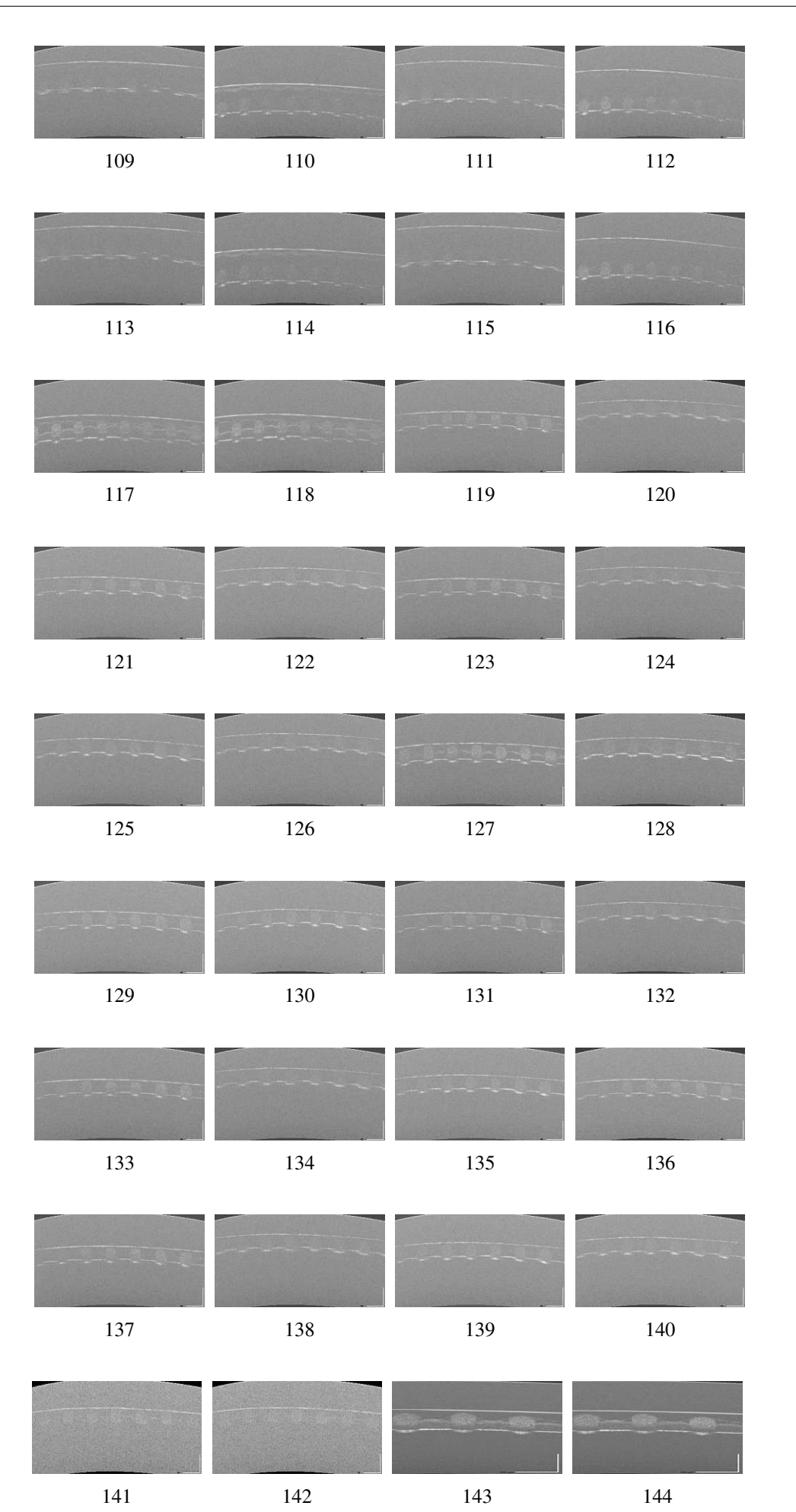
A3: OCT images: main tests



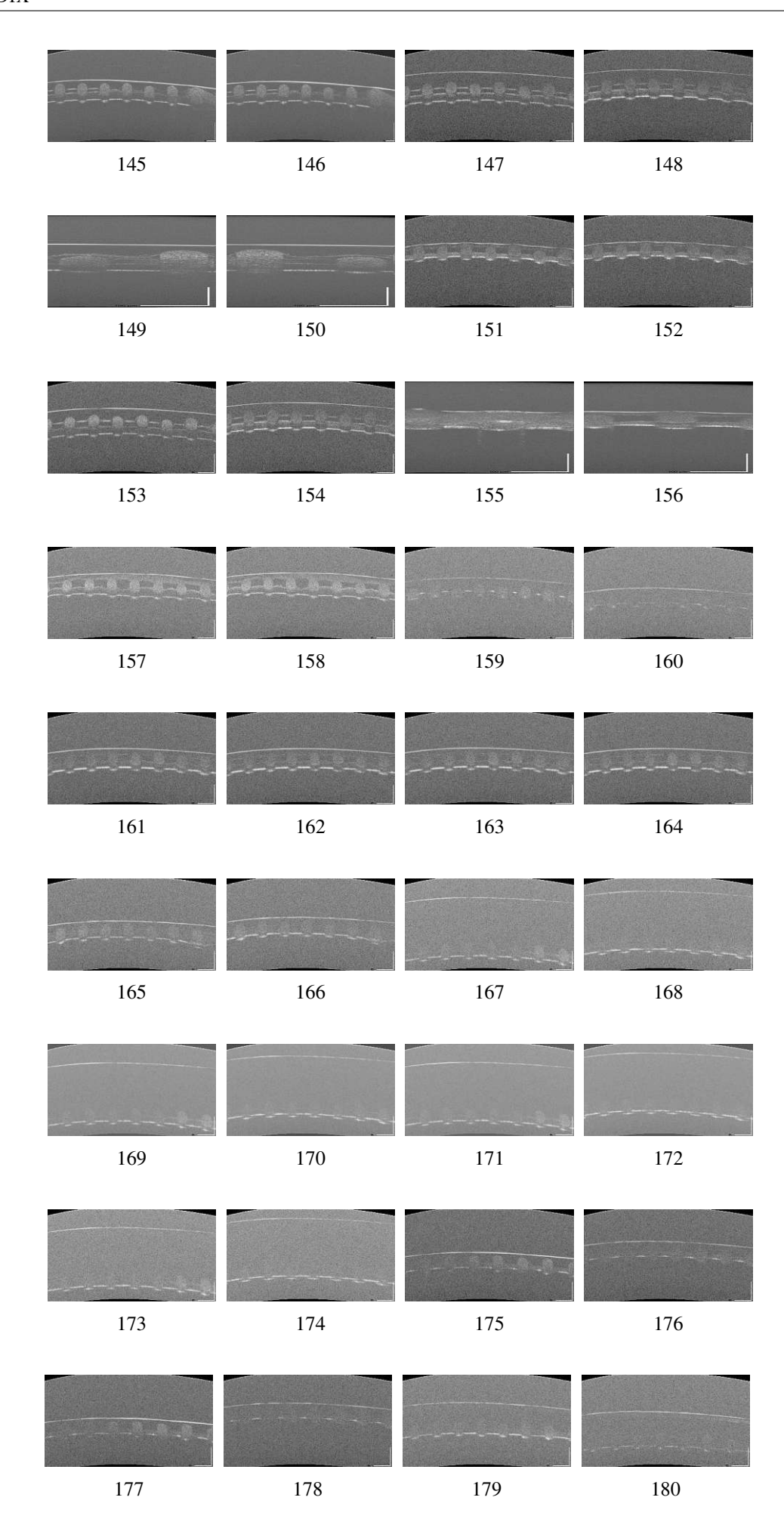
xxi



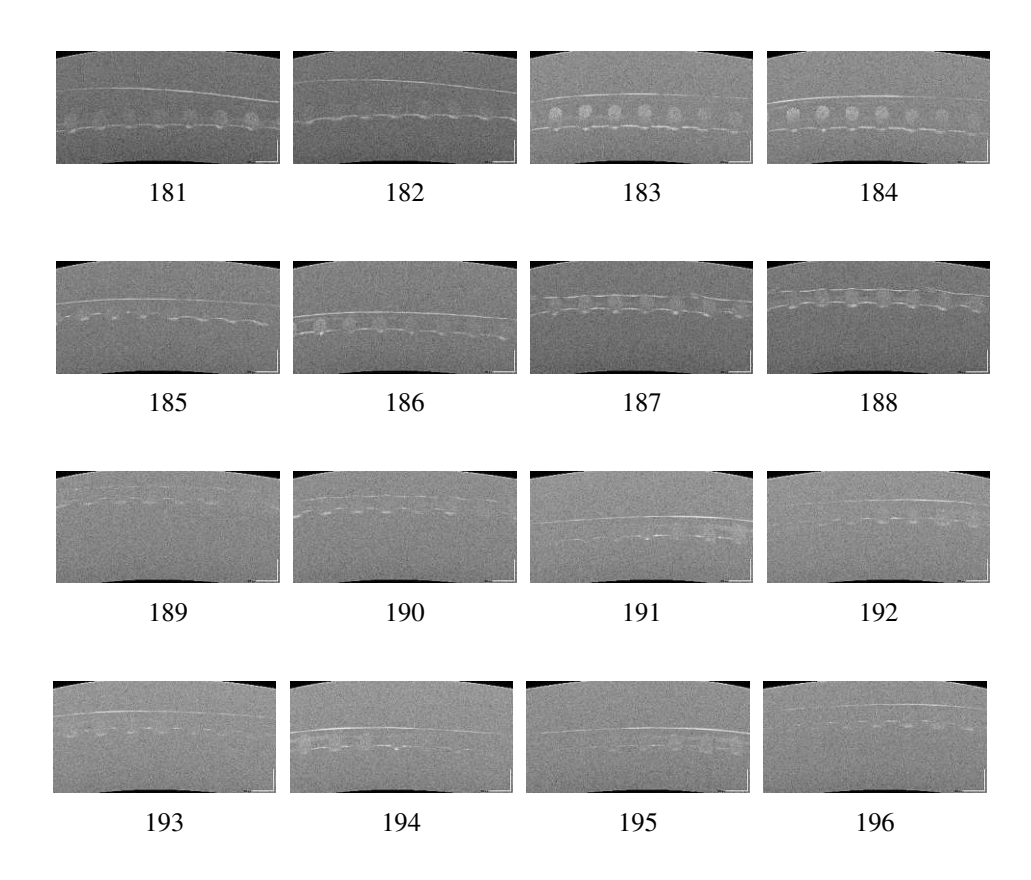
xxii



xxiii

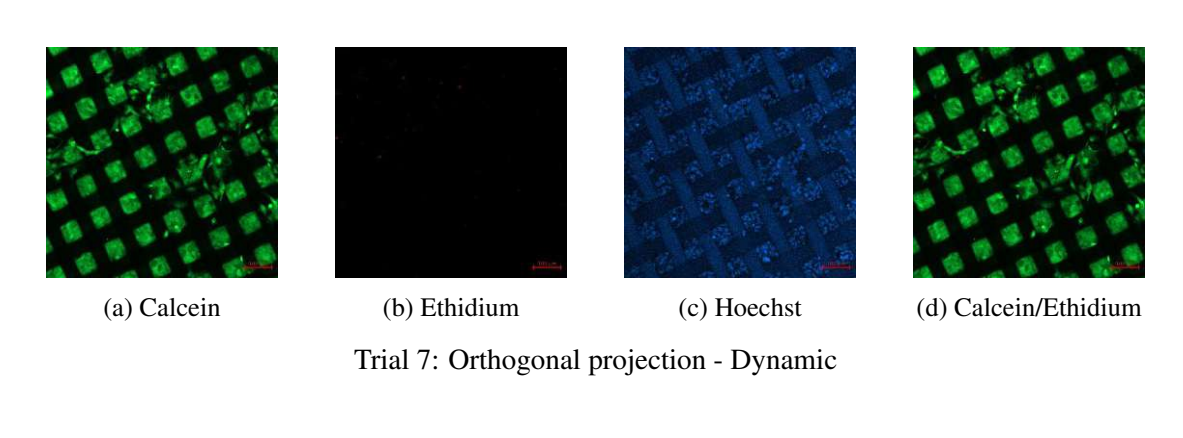


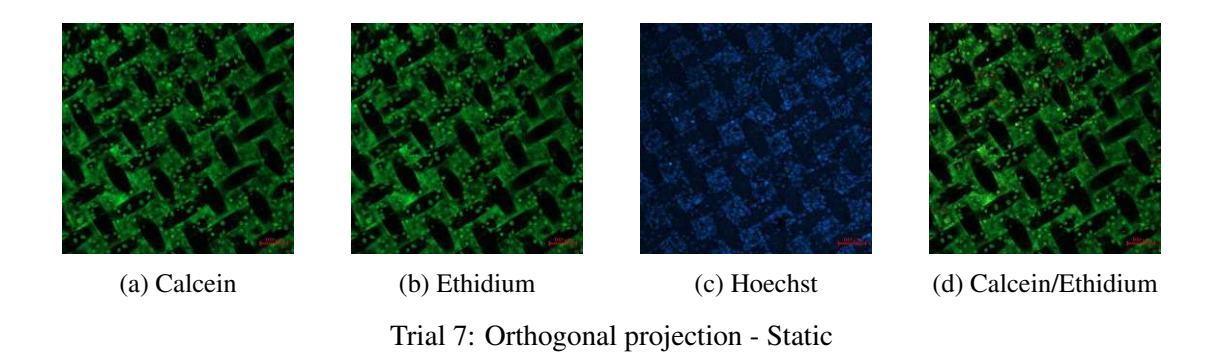
xxiv

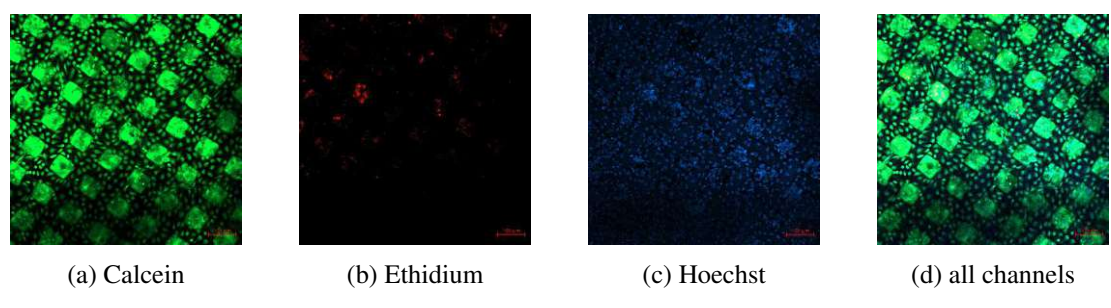


A.7 Viability

Orthogonal Projections A.7.1



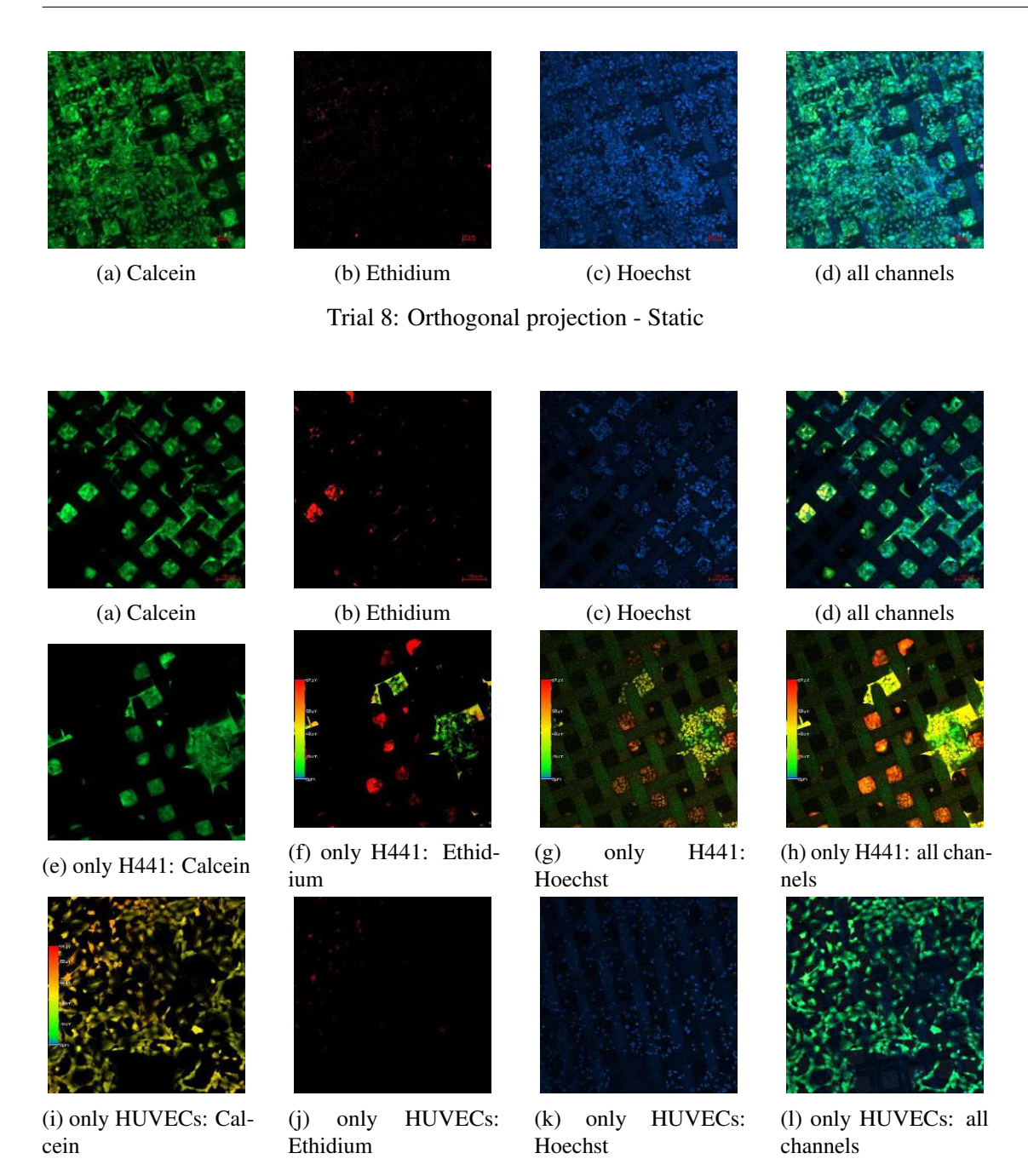




Trial 8: Orthogonal projection - Dynamic

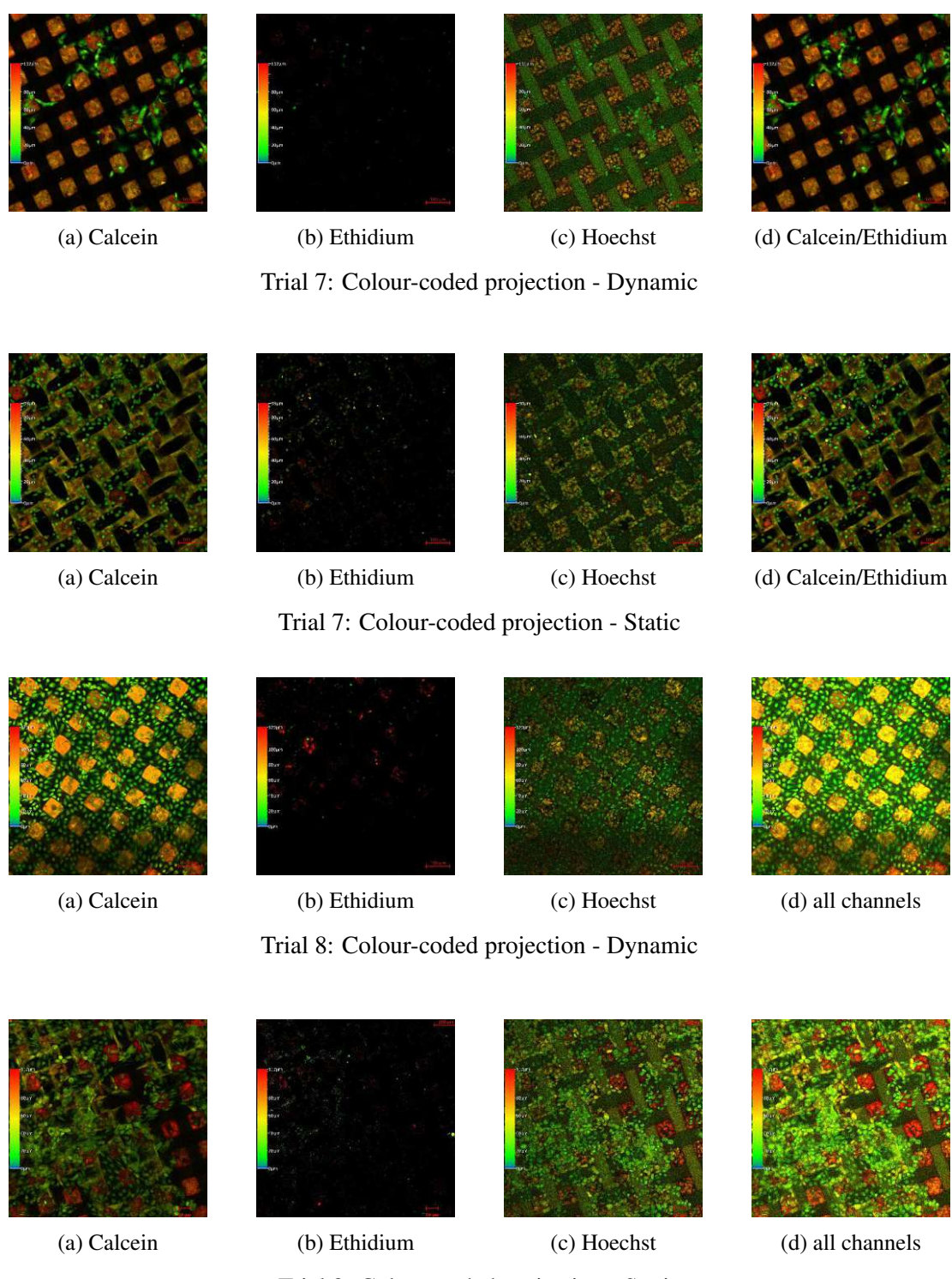
xxvi





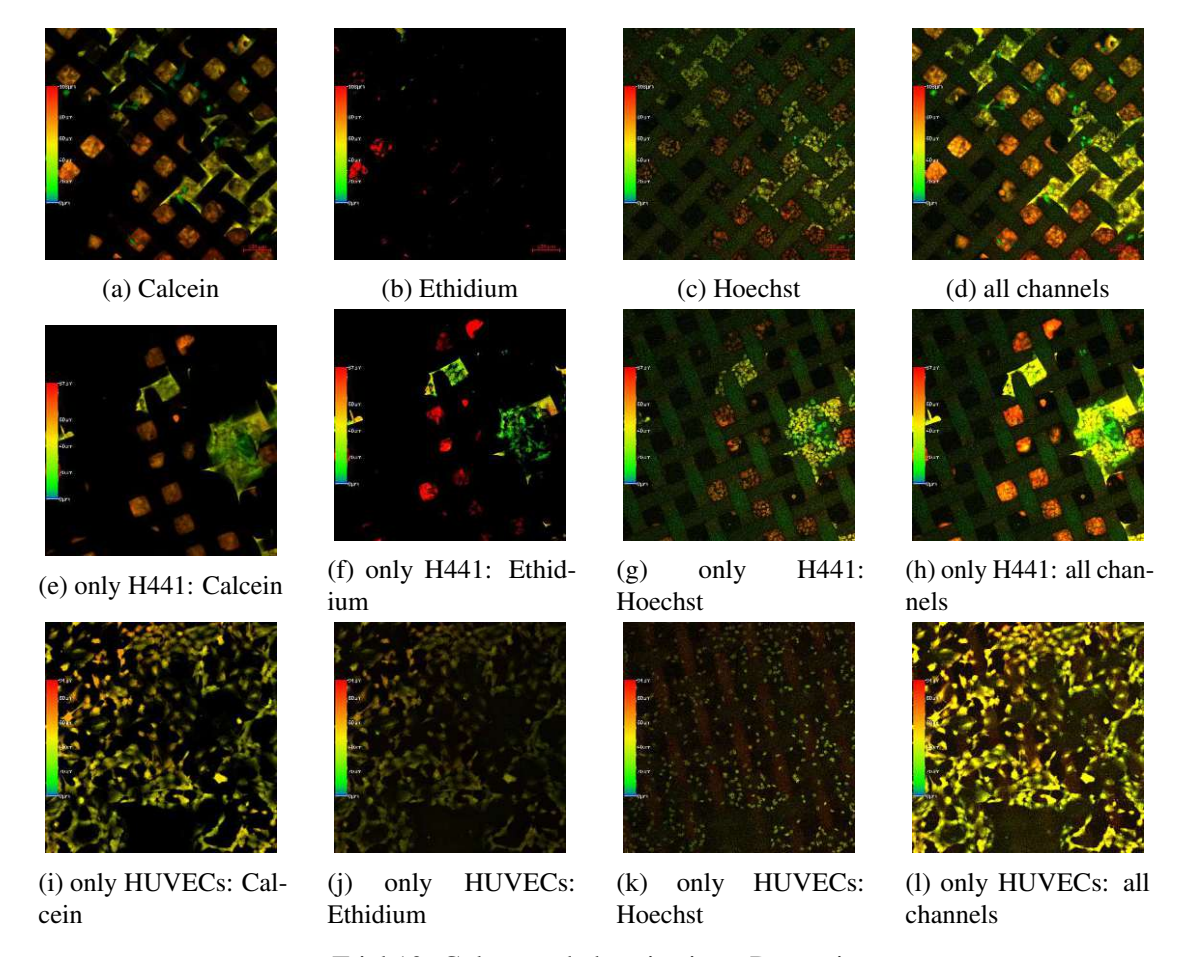
Trial 10: Orthogonal projection - Dynamic

A.7.2 **Colour-Coded Projections**



Trial 8: Colour-coded projection - Static

xxviii



Trial 10: Colour-coded projection - Dynamic

List of Figures

xxxi

1.1	Overview: Dimension and importance of tissue stiffness	
1.2	Experiment conditions during cyclic breathing	5
1.3	Box 0: Theses	6
1.4	Schematic overview of experiment set-up and schedule	8
2.1	Schematic overview: Biological membrane	9
2.2	Schema of double membrane coated on mesh of well	10
2.3	Schematic overview: Breathing phase	10
2.4	Set-up of chip for breathing	12
2.5	Principle of OCT	13
2.6	OCT protocol	15
2.7	Derivation of the Formula for Strain Calculation	16
2.8	Spherical cap geometry used to calculate stress and strain in the bulge test	17
2.9	Pathway of Processing OCT data	19
2.10	FITC-method as viability assay	20
2.11	Principle of Confocal Laser Scanning Microscopy	22
3.1	First OCT capture	26
3.2	Trial 4: OCT cross-section and external OCT camera image	26
3.3	Deflection image of the coated membrane during dynamic loading (Trial 4)	27
3.4	Deflection measurement of the biological membrane	27
3.5	Trial 11: OCT images Dynamic	30
3.6	Trial 11: OCT images Static and Control	31
3.7	Trials 8-11: OCT images Heterogeneity	32
3.8	Abstracted trends of mechanical response	34
3.9	Welch's test: Individual values with Mean and SD by groups	36
3.10	Welch's test: Individual values with Mean and SD by trial	36
3.11	Trial 10: Orthogonal projection - Dynamic	37

3.12	Trial 10: Colour-coded projection - Dynamic	38
3.13	Sample overview: Viability assay	38
4.1	Box 1: Parameter Trends: Breathing system to Membrane	39
4.2	Box 2: Summary: OCT	40
4.3	Box 3: Summary: Permeability	41
4.4	Box 4: Summary: Viability	42
5.1	Box 5: Theses review	45
5.2	Box 6: Cross-Methodological Summary	47
A1	Microscopy images of coatings and cells	V
A2	OCT images: pre-tests	xiii
A3	OCT images: main tests	XX

List of Tables

2.1	Fluorescent reagents used for cell viability staining	22
3.1	Overview of experimental trials and methods of analysis	25
3.2	Parameters breathing	29
3.3	Summary of observations from mechanical stimulation experiments	34
3.4	FITC concentration data [$\mu g m L^{-1}$] across trials	35
3.5	Welch's <i>t</i> -test Results	36
3.6	Mixed-Effects Model Results (Identical Conditions Only)	37
A .1	OCT pre-tests: Filename conversion	xii
A.2	Overview of trial conditions and corresponding file references	xiv
A 3	OCT main tests: Filename conversion	xiv



Glossary

BPM Breaths per minute [min⁻¹]. 11

Breathing system MPS Stimulus by Fraunhofer Institute for Material and Beam Technology (IWS) to apply organotypic air pressure. 11

CE Collagen-Elastin. 3

CLSM Confocal Laser Scanning Microscopy. 21

EAH Ernst-Abbe-Hochschule Jena. 14, 18

ECM Extra-Cellular Matrix. 3

Filter TRAKETCH® adhesiveVENTpad PET 0.4 D7.0/3.0 by SABEU. 11

FITC Fluoresceinisothiocyanat. 20

OCT Optical Coherence Tomography. 7, 12

PBS Phosphate-buffered saline. 20

UKJ Universitätsklinikum Jena. 7

Well Corning® 15 mm NetwellTM Insert with 74 μm Mesh Size Polyester Membrane, Sterile. 5

xxxiii

TU Sibliothek, WIEN Your knowledge hub

Bibliography

- T. R. Cox and J. T. Erler, "Remodeling and homeostasis of the extracellular matrix: implications for fibrotic diseases and cancer," Disease Models & Mechanisms, vol. 4, pp. 165–178, Mar. 2011.
- G. Wells. "The [2] R. role of matrix stiffness in regulating behav-Hepatology, vol. 47, 4, 1394-1400, 2008. _eprint: https://onlinelibrary.wiley.com/doi/pdf/10.1002/hep.22193.
- P. Zamprogno, S. Wüthrich, S. Achenbach, G. Thoma, J. D. Stucki, N. Hobi, N. Schneider-Daum, C.-M. Lehr, H. Huwer, T. Geiser, R. A. Schmid, and O. T. Guenat, "Secondgeneration lung-on-a-chip with an array of stretchable alveoli made with a biological membrane," Communications Biology, vol. 4, pp. 1-10, Feb. 2021. Publisher: Nature Publishing Group.
- U. S. Epa and others, "Exposure factors handbook," Office of research and Development, Washington, DC, vol. 20460, pp. 2–6, 2011.
- H. Zhang, J. M. Penninger, Y. Li, N. Zhong, and A. S. Slutsky, "Angiotensin-converting enzyme 2 (ACE2) as a SARS-CoV-2 receptor: molecular mechanisms and potential therapeutic target," Intensive Care Medicine, vol. 46, pp. 586-590, Apr. 2020.
- P. Gehr, M. Bachofen, and E. R. Weibel, "The normal human lung: ultrastructure and morphometric estimation of diffusion capacity," Respiration Physiology, vol. 32, pp. 121– 140, Feb. 1978.
- [7] L. Knudsen and M. Ochs, "The micromechanics of lung alveoli: structure and function of surfactant and tissue components," Histochemistry and Cell Biology, vol. 150, no. 6, pp. 661-676, 2018.

3ibliothek, Die WIEN Your knowledge hub

- [8] E. R. Weibel, "On the tricks alveolar epithelial cells play to make a good lung," *American journal of respiratory and critical care medicine*, vol. 191, pp. 504–513, Mar. 2015. Num Pages: 10 Number: 5 Publisher: American Lung Association.
- [9] K. H. Benam, R. Villenave, C. Lucchesi, A. Varone, C. Hubeau, H.-H. Lee, S. E. Alves, M. Salmon, T. C. Ferrante, J. C. Weaver, A. Bahinski, G. A. Hamilton, and D. E. Ingber, "Small airway-on-a-chip enables analysis of human lung inflammation and drug responses in vitro," *Nature Methods*, vol. 13, pp. 151–157, Feb. 2016. Publisher: Nature Publishing Group.
- [10] A. O. Stucki, J. D. Stucki, S. R. R. Hall, M. Felder, Y. Mermoud, R. A. Schmid, T. Geiser, and O. T. Guenat, "A lung-on-a-chip array with an integrated bio-inspired respiration mechanism," *Lab on a Chip*, vol. 15, pp. 1302–1310, Feb. 2015. Publisher: The Royal Society of Chemistry.
- [11] D. Huh, B. D. Matthews, A. Mammoto, M. Montoya-Zavala, H. Yuan Hsin, and D. E. Ingber, "Reconstituting Organ-Level Lung Functions on a Chip," *Science (New York, N.Y.)*, vol. 328, pp. 1662–1668, June 2010.
- [12] S. N. Bhatia and D. E. Ingber, "Microfluidic organs-on-chips," *Nature Biotechnology*, vol. 32, pp. 760–772, Aug. 2014.
- [13] E. Roan and C. M. Waters, "What do we know about mechanical strain in lung alveoli?," *American Journal of Physiology Lung Cellular and Molecular Physiology*, vol. 301, pp. L625–L635, Nov. 2011.
- [14] S. E. Dunsmore and D. E. Rannels, "Extracellular matrix biology in the lung," *American Journal of Physiology-Lung Cellular and Molecular Physiology*, vol. 270, pp. L3–L27, Jan. 1996. Publisher: American Physiological Society.
- [15] D. Sicard, A. J. Haak, K. M. Choi, A. R. Craig, L. E. Fredenburgh, and D. J. Tschumperlin, "Aging and anatomical variations in lung tissue stiffness," *American Journal of Physiology Lung Cellular and Molecular Physiology*, vol. 314, pp. L946–L955, June 2018.
- [16] F. S. A. Cavalcante, S. Ito, K. Brewer, H. Sakai, A. M. Alencar, M. P. Almeida, J. S. Andrade, A. Majumdar, E. P. Ingenito, and B. Suki, "Mechanical interactions between collagen and proteoglycans: implications for the stability of lung tissue," *Journal of Applied Physiology (Bethesda, Md.: 1985)*, vol. 98, pp. 672–679, Feb. 2005.

xxxvi

- [17] B. Sapoval, M. Filoche, and E. R. Weibel, "Smaller is better-but not too small: a physical scale for the design of the mammalian pulmonary acinus," *Proceedings of the National Academy of Sciences of the United States of America*, vol. 99, pp. 10411–10416, Aug. 2002.
- [18] B. Suki, D. Stamenovic, and R. Hubmayr, "Lung Parenchymal Mechanics," *Comprehensive Physiology*, vol. 1, pp. 1317–1351, July 2011.
- [19] J. Mead, T. Takishima, and D. Leith, "Stress distribution in lungs: a model of pulmonary elasticity," *Journal of Applied Physiology*, vol. 28, pp. 596–608, May 1970.
- [20] J. Grune, A. Tabuchi, and W. M. Kuebler, "Alveolar dynamics during mechanical ventilation in the healthy and injured lung," *Intensive Care Medicine Experimental*, vol. 7, p. 34, July 2019.
- [21] B. E. Bouma, J. F. de Boer, D. Huang, I.-K. Jang, T. Yonetsu, C. L. Leggett, R. Leitgeb, D. D. Sampson, M. Suter, B. J. Vakoc, M. Villiger, and M. Wojtkowski, "Optical coherence tomography," *Nature Reviews Methods Primers*, vol. 2, pp. 1–20, Oct. 2022. Publisher: Nature Publishing Group.
- [22] S. Behrens, J. Golde, Y. Schöps, C. Polk, G. Seidel, F. Goerke, F. Sonntag, and F. Schmieder, "Mechanical stimulation and monitoring of artificial collagen membranes for Organ-on Chip applications: Towards 3D inline elastography based on optical coherence tomography," *Current Directions in Biomedical Engineering*, vol. 10, no. 4, pp. 70–73, 2024. Publisher: Walter de Gruyter GmbH.
- [23] Y. B. Arık, A. de sa Vivas, D. Laarveld, N. van Laar, J. Gemser, T. Visscher, A. van den Berg, R. Passier, and A. D. van der Meer, "Collagen I Based Enzymatically Degradable Membranes for Organ-on-a-Chip Barrier Models," ACS Biomaterials Science & Engineering, vol. 7, pp. 2998–3005, July 2021.
- [24] P. Zamprogno, G. Thoma, V. Cencen, D. Ferrari, B. Putz, J. Michler, G. E. Fantner, and O. T. Guenat, "Mechanical Properties of Soft Biological Membranes for Organ-on-a-Chip Assessed by Bulge Test and AFM," ACS Biomaterials Science & Engineering, vol. 7, pp. 2990–2997, July 2021. Publisher: American Chemical Society.
- [25] Beams, structure and properties of thin films. john wiley & sons, inc., 1959.
- [26] M. K. Small and W. D. Nix, "Analysis of the accuracy of the bulge test in determining the mechanical properties of thin films," *Journal of Materials Research*, vol. 7, pp. 1553–1563, June 1992.

IV Sibliothek, Die app WIEN Your knowledge hub

- [27] I. Hubatsch, E. G. E. Ragnarsson, and P. Artursson, "Determination of drug permeability and prediction of drug absorption in Caco-2 monolayers," *Nature Protocols*, vol. 2, pp. 2111–2119, Sept. 2007. Publisher: Nature Publishing Group.
- [28] "ZEISS LSM 900 Confocal for Materials Research."
- [29] "LIVE/DEADTM Viability/Cytotoxicity Kit, for mammalian cells."
- [30] P. Thurner, "Tissue Biomechanics 317.026, VO, SS2023 Collagen fibril structure, assembly and mechanics," 2023.
- [31] M. Achilli and D. Mantovani, "Tailoring Mechanical Properties of Collagen-Based Scaffolds for Vascular Tissue Engineering: The Effects of pH, Temperature and Ionic Strength on Gelation," *Polymers*, vol. 2, pp. 664–680, Dec. 2010. Number: 4 Publisher: Molecular Diversity Preservation International.
- [32] O. Bronner-Shtrauchler, E. Nativ-Roth, D. S. Sanchez, M. Zaiden, and N. Vidavsky, "Multimodal characterization of the collagen hydrogel structure and properties in response to physiologically relevant pH fluctuations," *Acta Biomaterialia*, vol. 178, pp. 170–180, Apr. 2024.

xxxviii